J. Fluid Mech. (1984), *vol.* 148, *pp.* 155–191
Printed in Great Britain

Pressure spectra in turbulent free shear flows

By WILLIAM K. GEORGE,
State University of New York at Buffalo, Amherst, New York 14260

PAUL D. BEUTHER
Owens Corning Fiberglas Co. Technical Center, Granville, Ohio 43023

AND ROGER E. A. ARNDT
University of Minnesota, Minneapolis, Minnesota 55414

(Received 13 September 1976 and in revised form 1 May 1984)

Spectral models for turbulent pressure fluctuations are developed by directly Fourier transforming the integral solution to the Poisson equation for a homogeneous constant-mean-shear flow. The turbulence–turbulence interaction is seen to possess the well-known $k^{-\frac{7}{3}}$ inertial subrange and to dominate the high-wavenumber region. The turbulence–mean-shear contribution is seen to be dominant in the energy-containing range and falls off as $k^{-\frac{11}{3}}$ in the inertial subrange. The subrange constants and the mean-square pressure fluctuation are evaluated using a spectral model for the velocity. A spectral analysis of the velocity contamination of a pressure probe is also presented. Results are compared with spectral measurements with a static-pressure probe in the mixing layer of an axisymmetric jet.

PART 1. THEORETICAL DEVELOPMENT

1. Introduction

The problem of pressure fluctuations in a turbulent flow has been the subject of numerous investigations over the past fifty years. Taylor (1935, 1936) used dimensional and physical arguments to estimate the mean-square fluctuating pressure gradient in an isotropic turbulent flow. Heisenberg (1948) used the Millionshchikov hypothesis (fourth moments are related to second moments as though they were normally distributed random variables) to obtain an integral expression for the fluctuating pressure gradient in isotropic turbulence which depended on the velocity spectrum function $E(k)$. Similar approaches were taken by Chandrasekhar (1949), who improved Heisenberg's calculation, by Batchelor (1951), who obtained a similar integral for the mean-square fluctuating pressure as well as one involving the velocity correlations, and by Obukhov (1949) and Yaglom (1949), who calculated the structure function for the fluctuating pressure. From this work it was deduced that in isotropic flow the maximum contribution to the mean-square pressure fluctuation was from wavenumbers near the maximum of $E(k)$; that is, from wavenumbers in the energy-containing range. The primary contributions to the pressure-gradient fluctuations came from neither the energy-containing range nor from the dissipative range, but from an intermediate range of wavenumbers where $kE(k)$ is a maximum.

Other attempts to estimate the mean-square pressure fluctuation from the formulation in terms of the velocity correlations were made by Uberoi (1953), Kraichnan (1956) and Hinze (1959). Uberoi used measured second-order velocity

correlations in isotropic flow as did Batchelor, but with more extensive data. Uberoi also showed the validity of the Millionshchikov hypothesis for his data. Kraichnan and Hinze used Gaussian and simple exponential decay functions to represent the velocity correlation empirically. The result of the latter, $B_{LL}(r) \approx \exp(-|r|/l)$, yielded $\overline{p^2} \approx 0.5\rho^2(\overline{u^2})^2$, which was nearly equal to that deduced by Uberoi from experimental velocity data. Other contributors to the understanding of pressure fluctuations in isotropic turbulent flow included Obukhov & Yaglom (1951) and Golitzin (1963). A detailed discussion of these contributions is contained in Monin & Yaglom (1975). Kraichnan (1956) also attempted to assess the effect of anisotropy on the mean-sqaure pressure fluctuations, and was able to show that a reduction could be expected.

There were no attempts reported to calculate a spectrum for the pressure fluctuations, perhaps because of difficulties in integrating the difficult integral expressions. Inoue (1951) and Batchelor (1953) did note on dimensional grounds that the spectrum of the pressure fluctuations in the inertial subrange was given by $\pi(k)/\rho^2 \propto \epsilon^{\frac{4}{3}}k^{-\frac{7}{3}}$, where ϵ is the rate of dissipation of energy per unit mass and $\pi(k)$ is the pressure-spectrum function.

Attempts to address the difficult problem of pressure fluctuations in free turbulent shear flows appear to be limited to the efforts of Kraichnan (1956) and Lilley (1956). By decomposing the velocity field into mean and fluctuating parts and ignoring third-order velocity moments, they were able to identify two source terms: a turbulence–mean-shear contribution and a turbulence–turbulence contribution. The latter contribution (with the assumption of isotropy) was identical with that discussed above, while the former was integrated by assuming a uniform mean shear and homogeneous turbulent field. Kraichnan, using an isotropic model, calculated the contribution to the mean-square pressure fluctuation from the mean-shear term as

$$\frac{1}{\rho^2}\overline{p^2} \approx 0.53\overline{u^2}l^2\left(\frac{\mathrm{d}U}{\mathrm{d}y}\right)^2, \tag{1.1}$$

where l was the integral scale for the assumed exponentially decaying velocity correlation. Anisotropy was again shown to reduce the coefficient.

Except for the work of Jones *et al.* (1979) and our own (George 1974; George & Beuther 1977; George, Beuther & Arndt 1980; Beuther, George & Arndt 1977*a*,*b*), there appears to have been no effort to calculate the form of the pressure spectrum in a turbulent shear flow. This paper attempts to redress this neglect by calculating explicit forms for the various contributions to the pressure spectrum in the inertial subrange in a free shear flow. The results are believed to be applicable at an intermediate range of wavenumbers in a variety of turbulent shear flows and provide a basis for evaluation of recent attempts to measure pressure spectra in such flows.

In §§2–11 the spectral solution to the Poisson equation for the pressure will be derived and decomposed into terms directly dependent on the mean shear and terms depending only on fluctuating quantities. The wavenumber dependence of these terms will be deduced from dimensional considerations, and explicit values for the coefficients will be calculated from an assumed model for the velocity spectrum. Finally the mean-square fluctuating pressure and pressure gradient will be evaluated and compared with the previously cited results. A comparison of experimental data with the theory presented here, and the evaluation of the experimental techniques is presented in Part 2 (§§12–19).

2. The Poisson equation for the pressure, and its solution for turbulent free shear flows

It is well known that the governing equation for the static pressure field in an incompressible fluid can be derived from the momentum and mass-conservation equations as

$$\frac{1}{\rho}\nabla^2\tilde{p} = -\frac{\partial\tilde{u}_i}{\partial x_j}\frac{\partial\tilde{u}_j}{\partial x_i}, \tag{2.1}$$

where ∇^2 is the Laplacian operator, $\tilde{p}$ represents the instantaneous static pressure, ρ is the density and $\tilde{u}_i$ is the instantaneous velocity vector. This equation can be integrated for a variety of situations using the appropriate Green functions.

If we confine our attention to free shear flows (no boundaries) the surface-integral term vanishes and we can write

$$\tilde{p}(\boldsymbol{x},t) = -\frac{\rho}{4\pi}\int\left[\frac{\partial\tilde{u}_i}{\partial y_j}\frac{\partial\tilde{u}_j}{\partial y_i}\right]\frac{\mathrm{d}^3\boldsymbol{y}}{|\boldsymbol{y}-\boldsymbol{x}|}, \tag{2.2}$$

where, unless otherwise denoted, $\int$ refers to a volume integral over all space. Decomposing the velocity and pressure fields into mean and fluctuating parts, we can write for the fluctuating static pressure (cf. Townsend 1976)

$$\begin{aligned}\frac{1}{\rho}p(\boldsymbol{x},t) &= \frac{1}{\rho}[\tilde{p}(\boldsymbol{x},t)-P(\boldsymbol{x},t)]\\ &= -\frac{1}{4\pi}\int\left[\frac{\partial U_i}{\partial y_j}\frac{\partial u_j}{\partial y_i}+\frac{\partial U_j}{\partial y_i}\frac{\partial u_i}{\partial y_j}\right]\frac{\mathrm{d}^3\boldsymbol{y}}{|\boldsymbol{y}-\boldsymbol{x}|}-\frac{1}{4\pi}\int\frac{\partial^2}{\partial y_i\partial y_j}[u_iu_j-\overline{u_iu_j}]\frac{\mathrm{d}^3\boldsymbol{y}}{|\boldsymbol{y}-\boldsymbol{x}|},\end{aligned} \tag{2.3}$$

where lower-case letters are used to indicate fluctuating values and capitals to indicate mean quantities. It is clear that there are two different mechanisms for generating turbulent pressure fluctuations: an interaction of the turbulence with the mean shear and an interaction of the turbulence with itself.

We define the cross-correlation of the pressure fluctuations at two points in space as

$$B_{p,p}(\boldsymbol{x},\boldsymbol{x}') = \overline{p(\boldsymbol{x})\,p(\boldsymbol{x}')}. \tag{2.4}$$

Using primed values to indicate that the variable is to be evaluated at position $\boldsymbol{y}'$, it is straightforward to show that

$$\begin{aligned}&\frac{1}{\rho^2}[B_{p,p}(\boldsymbol{x},\boldsymbol{x}')]\\ &= \frac{1}{(4\pi)^2}\int\int\left\{\left[\frac{\partial U_i}{\partial y_j}\frac{\partial U'_l}{\partial y'_m}\frac{\partial^2\overline{u_ju'_m}}{\partial y_i\partial y'_l}+\frac{\partial U_i}{\partial y_j}\frac{\partial U'_m}{\partial y'_l}\frac{\partial^2\overline{u_ju'_l}}{\partial y_i\partial y'_m}+\frac{\partial U_j}{\partial y_i}\frac{\partial U'_l}{\partial y'_m}\frac{\partial^2\overline{u_iu'_m}}{\partial y_j\partial y'_l}+\frac{\partial U_j}{\partial y_i}\frac{\partial U'_m}{\partial y'_l}\frac{\partial^2\overline{u_iu'_l}}{\partial y_j\partial y'_m}\right]\right.\\ &\quad+\left[\frac{\partial U_i}{\partial y_j}\frac{\partial^3\overline{u_ju'_lu'_m}}{\partial y_i\partial y'_l\partial y'_m}+\frac{\partial U_j}{\partial y_i}\frac{\partial^3\overline{u_iu'_lu'_m}}{\partial y_j\partial y'_l\partial y'_m}+\frac{\partial U'_l}{\partial y'_m}\frac{\partial^3\overline{u'_mu_iu_j}}{\partial y'_l\partial y_i\partial y_j}+\frac{\partial U'_m}{\partial y'_l}\frac{\partial^3\overline{u'_lu_iu_j}}{\partial y'_m\partial y_i\partial y_j}\right]\\ &\quad\left.+\left[\frac{\partial^4\overline{u_iu_ju'_lu'_m}}{\partial y_i\partial y_j\partial y'_l\partial y'_m}-\frac{\partial^2\overline{u_iu_j}}{\partial y_i\partial y_j}\frac{\partial^2\overline{u'_lu'_m}}{\partial y'\partial y'_m}\right]\right\}\frac{\mathrm{d}^3\boldsymbol{y}}{|\boldsymbol{y}-\boldsymbol{x}|}\frac{\mathrm{d}^3\boldsymbol{y}'}{|\boldsymbol{y}'-\boldsymbol{x}'|}.\end{aligned} \tag{2.5}$$

Equation (2.5) illustrates that there are two types of turbulence–mean-shear interactions that must be considered: those resulting from second-moment terms and those resulting from third-moment terms.

3. The pressure covariance for a constant-mean-shear, homogeneous turbulent flow

We now restrict ourselves to a unidirectional flow in which the mean shear is constant; that is,

$$U_i = Ky_2\delta_{i1}. \tag{3.1}$$

We further assume that the turbulence is homogeneous and define†

$$B_{i,j}(\boldsymbol{r}) = \overline{u_i(\boldsymbol{y})\,u_j(\boldsymbol{y}+\boldsymbol{r})}, \tag{3.2}$$

$$B_{i,lm}(\boldsymbol{r}) = \overline{u_i(\boldsymbol{y})\,u_l(\boldsymbol{y}+\boldsymbol{r})\,u_m(\boldsymbol{y}+\boldsymbol{r})} \tag{3.3}$$

and

$$B_{ij,lm}(\boldsymbol{r}) = \overline{u_i(\boldsymbol{y})\,u_j(\boldsymbol{y})\,u_l(\boldsymbol{y}+\boldsymbol{r})\,u_m(\boldsymbol{y}+\boldsymbol{r})} - \overline{u_i(\boldsymbol{y})\,u_j(\boldsymbol{y})}\;\overline{u_l(\boldsymbol{y}+\boldsymbol{r})\,u_m(\boldsymbol{y}+\boldsymbol{r})}. \tag{3.4}$$

Letting $\boldsymbol{y}' = \boldsymbol{y}+\boldsymbol{r}$ and using the homogeneity condition

$$B_{ij,m}(-\boldsymbol{r}) = B_{m,ij}(\boldsymbol{r}), \tag{3.5}$$

it is straightforward to show that

$$\begin{aligned}\frac{1}{\rho^2}B_{p,p}(\boldsymbol{\xi}) = {}& \frac{1}{(4\pi)^2}4K^2\int\!\!\int\frac{\partial^2 B_{2,2}(\boldsymbol{r})}{\partial r_1^2}\frac{\mathrm{d}^3\boldsymbol{y}}{|\boldsymbol{x}-\boldsymbol{y}|}\frac{\mathrm{d}^3\boldsymbol{r}}{|\boldsymbol{x}+\boldsymbol{\xi}-\boldsymbol{y}-\boldsymbol{r}|} \\ & + \frac{1}{(4\pi)^2}2K\int\!\!\int\frac{\partial^3}{\partial r_1\,\partial r_l\,\partial r_m}[B_{2,lm}(-\boldsymbol{r})-B_{2,lm}(\boldsymbol{r})]\frac{\mathrm{d}^3\boldsymbol{y}}{|\boldsymbol{x}-\boldsymbol{y}|}\frac{\mathrm{d}^3\boldsymbol{r}}{|\boldsymbol{x}+\boldsymbol{\xi}-\boldsymbol{y}-\boldsymbol{r}|} \\ & + \frac{1}{(4\pi)^2}\int\!\!\int\frac{\partial^4 B_{ij,lm}(\boldsymbol{r})}{\partial r_i\,\partial r_j\,\partial r_l\,\partial r_m}\frac{\mathrm{d}^3\boldsymbol{y}}{|\boldsymbol{x}-\boldsymbol{y}|}\frac{\mathrm{d}^3\boldsymbol{r}}{|\boldsymbol{x}+\boldsymbol{\xi}-\boldsymbol{y}-\boldsymbol{r}|}.\end{aligned} \tag{3.6}$$

4. The spectrum of the static pressure fluctuations

We can define the cross-spectral densities of the pressure and velocity moments as the three-dimensional Fourier transforms of the cross-correlations as follows:

$$F_{p,p}(\boldsymbol{k}) = \frac{1}{(2\pi)^3}\int\!\!\int\!\!\int_{-\infty}^{\infty} \mathrm{e}^{\mathrm{i}\boldsymbol{k}\cdot\boldsymbol{r}}B_{p,p}(\boldsymbol{r})\,\mathrm{d}^3\boldsymbol{r}, \tag{4.1}$$

$$F_{i,j}(\boldsymbol{k}) = \frac{1}{(2\pi)^3}\int\!\!\int\!\!\int_{-\infty}^{\infty} \mathrm{e}^{\mathrm{i}\boldsymbol{k}\cdot\boldsymbol{r}}B_{i,j}(\boldsymbol{r})\,\mathrm{d}^3\boldsymbol{r}, \tag{4.2}$$

$$F_{i,lm}(\boldsymbol{k}) = \frac{1}{(2\pi)^3}\int\!\!\int\!\!\int_{-\infty}^{\infty} \mathrm{e}^{\mathrm{i}\boldsymbol{k}\cdot\boldsymbol{r}}B_{i,lm}(\boldsymbol{r})\,\mathrm{d}^3\boldsymbol{r}, \tag{4.3}$$

$$F_{ij,lm}(\boldsymbol{k}) = \frac{1}{(2\pi)^3}\int\!\!\int\!\!\int_{-\infty}^{\infty} \mathrm{e}^{\mathrm{i}\boldsymbol{k}\cdot\boldsymbol{r}}B_{ij,lm}(\boldsymbol{r})\,\mathrm{d}^3\boldsymbol{r}. \tag{4.4}$$

By taking the transform of (3.6) and using (4.1)–(4.4), we can obtain the turbulence pressure spectrum as

$$\begin{aligned}\frac{1}{\rho^2}F_{p,p}(\boldsymbol{k}) = {}& \frac{K^2}{4\pi^2}[k_1^2\,F_{2,2}(\boldsymbol{k})\,W(\boldsymbol{k})] + \frac{K}{8\pi^2}\mathrm{i}k_1\,k_l\,k_m\,[F^*_{2,lm}(\boldsymbol{k})-F_{2,lm}(\boldsymbol{k})]\,W(\boldsymbol{k}) \\ & + \frac{1}{(4\pi)^2}k_i\,k_j\,k_l\,k_m\,F_{ij,lm}(\boldsymbol{k})\,W(\boldsymbol{k}),\end{aligned} \tag{4.5}$$

† We follow closely the notation of Monin & Yaglom (1975).

where * denotes the complex conjugate, and we have defined

$$W(\boldsymbol{k}) = \left| \int e^{i\boldsymbol{k}\cdot\boldsymbol{r}} \frac{d^3\boldsymbol{r}}{|\boldsymbol{r}|} \right|^2. \tag{4.6}$$

$W(\boldsymbol{k})$ is a wavenumber filter which weights the contributions of the different velocity Fourier components to the pressure spectrum. It is shown in the Appendix that

$$W(\boldsymbol{k}) = \frac{(4\pi)^2}{k^4}, \tag{4.7}$$

where $k = |\boldsymbol{k}|$. The rapid roll-off with increasing wavenumber shows that the pressure spectrum will be dominated by the larger turbulence scales.

Using this result, (4.5) can be rewritten as

$$\begin{aligned} \frac{1}{\rho^2} F_{p,p}(\boldsymbol{k}) = {} & 4K^2 \left[\frac{k_1^2}{k^4} F_{2,2}(\boldsymbol{k}) \right] \\ & \text{(2nd-moment turbulence–shear interaction)} \\ & + 2iK \left[\frac{k_1 k_l k_m}{k^4} (F^*_{2,lm}(\boldsymbol{k}) - F_{2,lm}(\boldsymbol{k}) \right] \\ & \text{(3rd-moment turbulence–shear interaction)} \\ & + \frac{k_i k_j k_l k_m}{k^4} F_{ij,lm}(\boldsymbol{k}) \\ & \text{(turbulence–turbulence interaction).} \end{aligned} \tag{4.8}$$

The last term, which represents the turbulence–turbulence interaction spectrum, is not new and has previously been given by Batchelor (1951) (for an excellent summary see Monin & Yaglom 1975). The second term involving the third-moment interaction with the mean shear can be shown to be exactly zero for an isotropic turbulent flow. Therefore, because of the local isotropy at high wavenumbers, one might expect it to be significant only at low wavenumbers in high-Reynolds-number flows. Since the second-moment interaction with the mean shear is directly dependent on the turbulent energy and the Reynolds stress, it is likely that this term will never be negligible in a turbulent shear flow. The integral of this term was the only shear-interaction term considered by Kraichnan (1956) in his analysis of the mean-square pressure fluctuations.

5. The inertial subrange: dimensional and physical analysis

To proceed analytically beyond (4.8) without making rather restrictive assumptions about the flow (e.g. isotropy) appears to be impossible in view of the lack of information about the velocity moments. Therefore it is especially valuable to see if some general statements about the shape of the pressure spectrum can be made on dimensional and physical grounds before continuing the analysis.

It has long been established (Kolmogorov 1941) that at high Reynolds numbers at wavenumbers sufficiently larger than those that govern the primary decay processes and at which energy is added (usually, the energy-containing eddies) the turbulent-energy spectrum possesses a universal equilibrium range where the only governing parameters are ϵ, the rate of dissipation of turbulent energy per unit mass, ν, the kinematic viscosity, and k, the wavenumber. At an intermediate range of wavenumbers sufficiently removed from the effects of both viscosity and the large

scales, if the turbulent Reynolds number is sufficiently high, one finds an inertial subrange in which the only parameters are ϵ and k.

If we introduce the velocity spectrum function defined by

$$E(k) = \frac{1}{2}\int\int F_{i,i}(\boldsymbol{k})\,\mathrm{d}\sigma(\boldsymbol{k}), \tag{5.1}$$

where the integral is over spherical shells of radius k, then it is easy to show from dimensional analysis that in the inertial subrange

$$E(k) = \alpha\epsilon^{\frac{2}{3}}k^{-\frac{5}{3}} \quad (k_0 \ll k \ll \eta^{-1}), \tag{5.2}$$

where α is the Kolmogorov constant† and ϵ is the rate of dissipation of turbulent energy per unit mass. k_0 is a wavenumber characteristic of the energy-containing wavenumbers, and η is the Kolmogorov microscale, which characterizes the dissipative scales and is defined by

$$\eta = \left(\frac{\nu^3}{\epsilon}\right)^{\frac{1}{4}}. \tag{5.3}$$

A spectrum function for the pressure can similarly be defined as

$$\pi_p(k) = \int\int F_{p,p}(\boldsymbol{k})\,\mathrm{d}\sigma(\boldsymbol{k}). \tag{5.4}$$

It follows from (4.8) that $\pi(k)$ is composed of three parts, and can be written as

$$\pi_p(k) = \pi_{s2}(k) + \pi_{s3}(k) + \pi_t(k), \tag{5.5}$$

where π_{s2} and π_{s3} represent the second-and third-moment turbulence–mean-shear interaction spectrum functions respectively, and π_t represents the turbulence–turbulence interaction spectrum function.

The inertial subrange form for each of these spectrum functions must be determined by only the parameters k, ϵ and K. Using the dependence on the mean shear given by (4.8), it follows immediately from dimensional analysis that

$$\frac{1}{\rho^2}\pi_{s2}(k) = \alpha_2 K^2\epsilon^{\frac{2}{3}}k^{-\frac{11}{3}}, \tag{5.6}$$

$$\frac{1}{\rho^2}\pi_{s3}(k) = \alpha_3 K\epsilon k^{-3}, \tag{5.7}$$

$$\frac{1}{\rho^2}\pi_t(k) = \alpha_p\epsilon^{\frac{4}{3}}k^{-\frac{7}{3}}. \tag{5.8}$$

α_2, α_3 and α_p are universal constants analogous to the Kolmogorov constant for the velocity spectrum.

Equation (5.8) for the turbulence–turbulence spectrum $\pi(k)$ appears to have first been suggested by Inoue (1951) and Batchelor (1953), although similar considerations for the pressure correlation function were given at slightly earlier dates by Heisenberg (1948) and Obukhov (1949). The forms for the shear-interaction spectra of (5.6) and (5.7) were first given by Beuther *et al.* (1977*a*,*b*) and by Jones *et al.* (1979).

Similar dimensional considerations for the fourth-order velocity spectra also lead to a $-\frac{7}{3}$ law (cf. Dutton & Deaven 1972). However, Van Atta & Wyngaard (1975) have recently shown these arguments for higher-order spectra to be inconsistent with the experimental data, where a $k^{-\frac{5}{3}}$ range is observed regardless of the order of the

† Throughout this paper we take $\alpha = 1.5$ (see Tennekes & Lumley 1972).

velocity spectrum. They explained this discrepancy by arguing that the spectrum of u^n must depend on the dissipation of u^n, say ϵ_n, as well as ϵ and k. Thus

$$E_{u^n}(k) \propto \epsilon_n \epsilon^{\frac{1}{3}} k^{-\frac{5}{3}}.$$

This is similar to arguments used by Corrsin (1951) to derive the inertial subrange of the spectrum of a passive scalar.

Since the pressure spectrum (the turbulence–turbulence interaction spectrum, in particular) depends on the fourth-order velocity spectra, it is necessary to ask which of these alternatives, $-\frac{7}{3}$ or $-\frac{5}{3}$, is appropriate. Later in this paper, we shall show that the $k^{-\frac{7}{3}}$ law is appropriate for the pressure spectrum of the turbulence–turbulence interactions, and is consistent with *both* the data and the arguments of Van Atta & Wyngaard. The physical reason for this is that there is no direct dissipation of pressure fluctuations.

In summary, we can state that the spectrum of the turbulent pressure fluctuations in the inertial subrange is the sum of three parts: a $k^{-\frac{11}{3}}$ component from the second-moment–shear interaction, a k^{-3} component from the third-moment–shear interaction, and a $k^{-\frac{7}{3}}$ component from the turbulence–turbulence interaction. Which of these dominates at any given wavenumber can be determined only if the mean-shear and turbulence quantities are given. However, it is clear that the turbulence–turbulence term will become relatively more important as we consider high wavenumbers. Moreover, it is important to note that all components of the pressure spectrum roll off faster than the $k^{-\frac{5}{3}}$ of the velocity spectra. Hence contamination of a pressure-sensitive probe by velocity signals could dominate at high wavenumbers. This subject will be addressed later.

6. The turbulence–mean-shear interaction pressure spectrum

From (4.8) the turbulence–mean-shear contribution to the pressure spectrum can be written as

$$\begin{aligned}\frac{1}{\rho^2} F^{\mathrm{ms}}_{p,p}(\boldsymbol{k}) &= \frac{1}{\rho^2} F^{\mathrm{ms1}}_{p,p}(\boldsymbol{k}) + \frac{1}{\rho^2} F^{\mathrm{ms2}}_{p,p}(\boldsymbol{k}) \\ &= 4K^2 \left[\frac{k_1^2}{k^4} F_{2,2}(\boldsymbol{k})\right] + 2\mathrm{i}K \frac{k_1 k_l k_m}{k^4} [F^*_{2,lm}(\boldsymbol{k}) - F_{2,lm}(\boldsymbol{k})]. \quad (6.1)\end{aligned}$$

If we had general forms for the velocity spectra $F_{2,2}$ and $F_{2,lm}$, we could immediately determine the pressure spectrum. Unfortunately, such forms are not available, and to proceed we must either use empirical equations or resort to assumptions of isotropy.

It is straightforward to show that the assumption of isotropy implies that the second term arising from third moments is identically zero. In view of the local isotropy at high wavenumbers, we expect the neglect of this term to be acceptable in all turbulent shear flows at high turbulent Reynolds number, at least in that range of wavenumbers corresponding to the universal-equilibrium range. Hereinafter, we will consider only the first term in (6.1), which involves only second-moment turbulence quantities.

For isotropic turbulent flow, a great deal is known about $E(k)$, the three-dimensional velocity spectrum function defined by (5.1). From isotropy (see Batchelor 1953) the three-dimensional velocity spectrum is given by

$$F_{i,j}(\boldsymbol{k}) = \frac{E(k)}{4\pi k^2} \left[\delta_{ij} - \frac{k_i k_j}{k^2}\right]. \quad (6.2)$$

Substituting this into (6.1) yields the turbulence–mean-shear interaction pressure spectrum as

$$\frac{1}{\rho^2}F^{\mathrm{ms}}_{p,p}(\boldsymbol{k}) = \frac{1}{\pi}K^2\frac{k_1^2}{k^6}E(k)\left[1-\frac{k_2^2}{k^2}\right]. \tag{6.3}$$

The contribution to the pressure spectrum function from the turbulence–mean-shear interaction can be obtained from its defining integral as

$$\pi_{\mathrm{s}}(k) = \int\int F^{\mathrm{ms1}}_{pp}(\boldsymbol{k})\,\mathrm{d}\sigma(\boldsymbol{k}), \tag{6.4}$$

where $\mathrm{d}\sigma(\boldsymbol{k})$ is an area element on a sphere of radius $k = |\boldsymbol{k}|$ and the integration is over the entire sphere. Substituting (6.3) into (6.4), transforming to spherical coordinates, and carrying out the integration yields

$$\pi_{\mathrm{s}}(k) = \tfrac{16}{15}K^2\frac{E(k)}{k^2}. \tag{6.5}$$

Although the spectrum function π_{s} is useful for theoretical considerations, it is the one-dimensional spectrum defined by

$$F^1_{p,p}(k_1) = \int\int_{-\infty}^{\infty} F_{p,p}(\boldsymbol{k})\,\mathrm{d}k_2\,\mathrm{d}k_3 \tag{6.6}$$

that is usually measured.

It follows immediately from (6.3) and (6.6) that the contribution of the turbulence–mean-shear interaction to the one-dimensional pressure spectrum is given by

$$\frac{1}{\rho^2}F^1_{pps}(k_1) = K^2\left\{k_1^2\int_{k_1}^{\infty}\frac{E(k)}{k^5}\,\mathrm{d}k + k_1^4\int_{k_1}^{\infty}\frac{E(k)}{k^7}\,\mathrm{d}k\right\}. \tag{6.7}$$

To calculate the spectrum function and the one-dimensional spectrum of the turbulence–mean–shear pressure fluctuations from (6.5) and (6.7) we need to assume a form for $E(k)$. It is well known that $E(k)$ has the following properties:

$$E(k) = \begin{cases} Ck^n & (k \text{ small}), \\ \alpha\epsilon^{\frac{2}{3}}k^{-\frac{5}{3}} & (\text{inertial subrange}) \end{cases} \tag{6.8}$$

(cf. Monin & Yaglom 1975). The exponent n is 4 if the flow is assumed to be both homogeneous and incompressible. If the constraint of homogeneity is relaxed, a value of 2 is appropriate. It is clear from (6.8) that the choice for n makes no difference at high wavenumbers. Thus, for isotropic flow, we choose the empirical spectrum suggested by von Kármán (1948) as

$$E(k) = \alpha\epsilon^{\frac{2}{3}}\lambda^{\frac{5}{3}}\frac{(k\lambda)^4}{[1+(k\lambda)^2]^{\frac{17}{6}}}, \tag{6.9}$$

where λ is chosen so that $E(k)$ integrates to yield the turbulent kinetic energy per unit mass $\frac{3}{2}u^2$. The velocity scale u is defined

$$u^2 = \tfrac{1}{3}[\overline{u_1^2}+\overline{u_2^2}+\overline{u_3^2}]. \tag{6.10}$$

For isotropic flow the relation between $E(k)$ and the one-dimensional velocity spectrum of the u_1 component is

$$F^1_{11}(k_1) = \frac{1}{2}\int_{k_1}^{\infty}\frac{E(k)}{k}\left[1-\frac{k_1^2}{k^2}\right]\mathrm{d}k. \tag{6.11}$$

Substituting (6.9) into (6.11) and carrying out the integration yields an $F_{11}^1(k)$, the one-dimensional von Kármán spectrum given as

$$F_{11}^1(k) = \tfrac{9}{55}\alpha\epsilon^{\frac{2}{3}}\frac{\lambda^{\frac{5}{3}}}{[1+(k\lambda)^2]^{\frac{5}{6}}}. \tag{6.12}$$

This is important since it provides the primary point of contact with the calculated results of Van Atta & Wyngaard discussed later.

By substituting (6.9) into (6.5) it is straightforward to show that $\pi_s(k) \to k^{-\frac{11}{3}}$ for large k, confirming the analysis of §5. The extent of the $k^{-\frac{11}{3}}$ region is, of course, limited by viscosity just as is the $k^{-\frac{5}{3}}$ region in the velocity spectrum. This could have been taken into account by choosing a form for $E(k)$ such as that proposed by Pao (1965), which cuts off exponentially above $k\eta \sim 0.15$. Since the turbulent–mean-shear spectrum cuts off so rapidly compared with the velocity spectrum this added complexity hardly seems warranted, even for calculations of the mean-square pressure gradient.

Figure 1 shows the turbulence–mean-shear pressure-spectrum function $\pi_s(k)$ calculated from (6.5) and (6.9). Figure 2 shows the calculated one-dimensional spectrum from (6.7) and (6.9). The calculated values are summarized in table 1. Both spectra have been normalized by the mean shear K, the rate of dissipation of turbulent energy per unit mass ϵ and the lengthscale l defined by

$$\epsilon = \frac{u^3}{l}. \tag{6.13}$$

By integrating (6.9) it can be shown that $\lambda = 0.96l$.

From (6.5) the coefficient of proportionality corresponding to the $k^{-\frac{11}{3}}$ range in the spectrum function for the turbulence–mean-shear interaction is seen to be $\frac{16}{15}\alpha \approx 1.07\alpha$. The corresponding range in the one-dimensional spectrum can be obtained directly from (6.7) as†

$$\frac{1}{\rho^2}F_{pps}^1(k_1) = 0.307\alpha K^2\epsilon^{\frac{2}{3}}k_1^{-\frac{11}{3}}. \tag{6.14}$$

It is interesting to note that this value is not $\frac{3}{22}$ times the spectrum-function coefficient, which would be expected from the isotropic relations for scalar spectra. This is because the turbulence–mean-shear pressure fluctuations are not isotropic even though the turbulence itself is assumed to be. It has already been noted that the constant of proportionality for the $k^{-\frac{2}{3}}$ range is identically zero, since we have assumed isotropic turbulence.

7. The turbulence–turbulence interaction pressure spectrum

From (4.8) the turbulence–turbulence interaction pressure spectrum is given by

$$\frac{1}{\rho^2}F_{p,p}^t(\boldsymbol{k}) = \frac{k_i k_j k_l k_m}{k^4}F_{ij,lm}(\boldsymbol{k}). \tag{7.1}$$

We follow Batchelor (1951) closely and assume that fourth-order moments of the turbulence can be related to second-order moments as though they were Gaussian (Millionshchikov 1941). We have

$$F_{ij,lm}(\boldsymbol{k}) = \int F_{i,l}(\boldsymbol{k}-\boldsymbol{k}')\,F_{j,m}(\boldsymbol{k}')\,\mathrm{d}^3\boldsymbol{k}' + \int F_{i,m}(\boldsymbol{k}-\boldsymbol{k}')\,F_{j,l}(\boldsymbol{k}')\,\mathrm{d}^3\boldsymbol{k}', \tag{7.2}$$

† Note that this must be multiplied by 2 to obtain the half-line spectrum value.

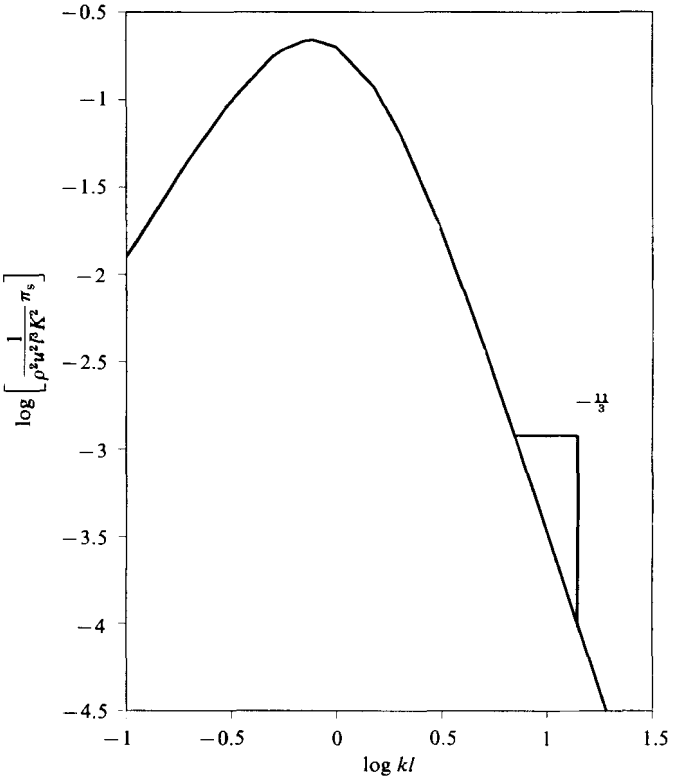

FIGURE 1. Turbulence–mean-shear pressure-spectrum function.

where a contribution at $\boldsymbol{k} = 0$ has been dropped. For isotropic turbulence this hypothesis is supported at moderate wavenumbers by the detailed measurements of Frenkiel & Klebanoff (1966) (see also Monin & Yaglom 1975), as well as by the spectral calculations of Van Atta & Wyngaard (1975).

By substituting (6.2) and (7.2) into (7.1), Batchelor's result is readily obtained as

$$\frac{1}{\rho^2}F^{\mathrm{t}}_{p,\,p}(\boldsymbol{k}) = \frac{1}{8\pi^2}\int E(\boldsymbol{k}')\,E(|\boldsymbol{k}-\boldsymbol{k}'|)\frac{\sin^4\phi}{|\boldsymbol{k}-\boldsymbol{k}'|^4}\,\mathrm{d}^3\boldsymbol{k}', \tag{7.3}$$

where ϕ is the angle between $\boldsymbol{k}$ and $\boldsymbol{k}'$.

To proceed beyond this point we assume the same empirical form for $E(k)$ as before. Substituting (6.9) into (7.3), transforming to spherical coordinates and integrating out the angular dependence yields

$$\frac{1}{\rho^2}F^{\mathrm{t}}_{p,\,p}(k) = \frac{1}{4\pi}\alpha^2\epsilon^{\frac{4}{3}}\lambda^{\frac{13}{3}}\int_0^\infty [G(k,k')\{(-\tfrac{6}{11})\,A_0\,x^{-\frac{11}{6}} - \tfrac{6}{5}A_1\,x^{-\frac{5}{6}} + 6A_2\,x^{\frac{1}{6}} + \tfrac{6}{7}A_3\,x^{\frac{7}{6}} + \tfrac{6}{13}A_4\,x^{\frac{13}{6}}\}\,|_{a-1}^{a+1}]\,\mathrm{d}k', \tag{7.4}$$

where $|_{a-1}^{a+1}$ means that the bracketed term is to be evaluated at these limits and where

$$A_0 = a^4 - 2a^2 + 1, \quad A_1 = -4a^3 + 4a, \quad A_2 = 6a^2 - 2, \quad A_3 = -4a, \quad A_4 = 1, \tag{7.5}$$

$$a = \frac{1+\lambda^2(k^2+k'^2)}{2kk'\lambda^2}, \tag{7.6}$$

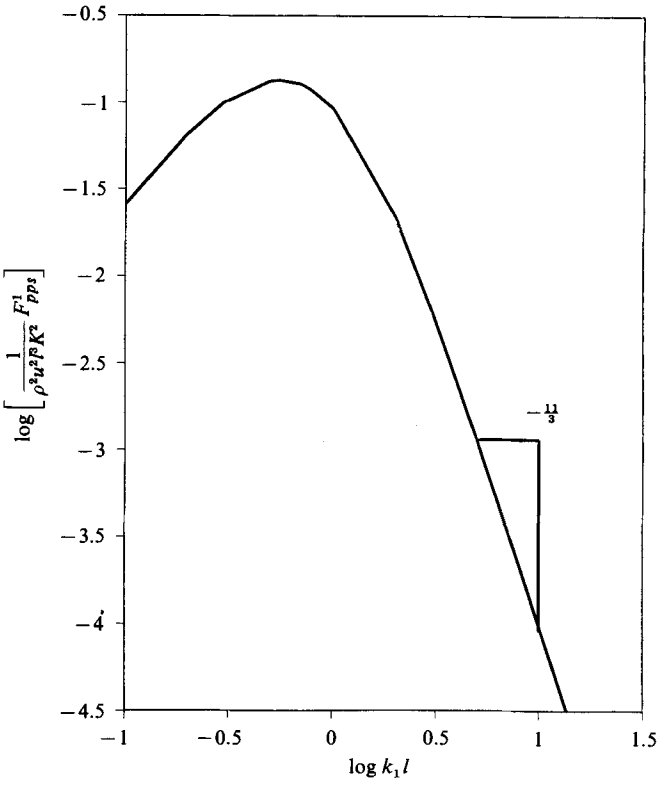

FIGURE 2. One-dimensional turbulence–mean-shear pressure spectrum.

kl	$\frac{1}{\rho^2 K^2 l^3 u^2}\pi_s$	$\frac{1}{\rho^2 K^2 l^3 u^2} F^1_{pps}$
0.10	1.25×10^{-2}	2.56×10^{-2}
0.20	4.60×10^{-2}	6.55×10^{-2}
0.30	9.13×10^{-2}	1.00×10^{-1}
0.50	1.77×10^{-1}	1.33×10^{-1}
0.55	1.91×10^{-1}	1.34×10^{-1}†
0.70	2.16×10^{-1}	1.27×10^{-1}
0.77	2.19×10^{-1}†	1.19×10^{-1}
1.0	1.99×10^{-1}	9.19×10^{-2}
2.0	6.38×10^{-2}	2.16×10^{-2}
3.0	2.06×10^{-2}	6.44×10^{-3}
5.0	3.88×10^{-3}	1.15×10^{-3}
7.0	1.20×10^{-3}	3.50×10^{-4}
10.0	3.34×10^{-4}	9.70×10^{-5}
20	2.69×10^{-5}	7.81×10^{-6}

† maximum value.

TABLE 1. Turbulence–mean-shear interaction spectrum

kl	$\frac{1}{\rho^2 u^4 l}\pi_t$	$\frac{1}{\rho^2 u^4 l}F^t_{ppt}$
0.1	3.50×10^{-4}	6.48×10^{-2}†
0.2	2.06×10^{-3}	6.46×10^{-2}
0.3	4.71×10^{-3}	6.41×10^{-2}
0.5	1.24×10^{-2}	6.23×10^{-2}
0.7	2.21×10^{-2}	5.96×10^{-2}
1	3.74×10^{-2}	5.46×10^{-2}
2	6.49×10^{-2}	3.60×10^{-2}
2.2	6.54×10^{-2}†	3.28×10^{-2}
3	5.95×10^{-2}	2.27×10^{-2}
5	3.53×10^{-2}	1.02×10^{-2}
7	2.09×10^{-2}	5.40×10^{-3}
10	1.08×10^{-2}	2.60×10^{-3}
20	2.55×10^{-3}	5.73×10^{-4}
30	1.04×10^{-3}	2.29×10^{-4}
50	3.26×10^{-4}	7.08×10^{-5}
70	1.50×10^{-4}	3.25×10^{-5}
100	6.61×10^{-5}	1.42×10^{-6}

† maximum value.

TABLE 2. Turbulence–turbulence interaction spectrum

$$G(k,k') = \frac{(k'\lambda)^6}{[1+(k'\lambda)^2]^{\frac{17}{6}}[2kk'\lambda^2]^{\frac{17}{6}}}. \tag{7.7}$$

Substituting (7.5)–(7.7) into (7.4), and rearranging the terms leads directly to the more convenient equation

$$\frac{1}{\rho^2}F^t_{p,\,p}(k) = \frac{2^{-\frac{17}{6}}}{4\pi}\alpha^2\epsilon^{\frac{4}{3}}\lambda^{\frac{13}{3}}[k\lambda]^{\frac{4}{3}}\int_0^\infty \mathrm{d}y\,\frac{y^{\frac{19}{6}}}{[1+(k\lambda)^2y^2]^{\frac{17}{6}}}I(a), \tag{7.8}$$

where $y = k'/k$ and $I(a)$ is defined by

$$I(a) = [\tfrac{186\,624}{5005}a^2 - \tfrac{1728}{143}][(a+1)^{\frac{1}{6}} - (a-1)^{\frac{1}{6}}] - \tfrac{31104}{5005}a[(a+1)^{\frac{1}{6}} + (a-1)^{\frac{1}{6}}]. \tag{7.9}$$

It is straightforward to show that, as $k\lambda\to\infty$, $I(a)\to I(y)$ only and that the contribution to the integral for $y \leqslant (k\lambda)^{-1}$ is negligible. Thus

$$\frac{1}{\rho^2}F^t_{p,\,p}(k)\to k^{-\frac{13}{3}} \quad \text{for large } k\lambda.$$

The spectrum function for the turbulence–turbulence interaction spectrum can be defined as before; from isotropy the result is

$$\pi_t(k) = 4\pi k^2 F^t_{p,\,p}(k). \tag{7.10}$$

It follows immediately from the asymptotic behaviour of $F^t_{p,\,p}$ that $\rho^{-2}\pi_t(k) \propto k^{-\frac{7}{3}}$ for large $k\lambda$ as already deduced in §5.

Equation (7.8) has been integrated numerically for a number of values of $k\lambda$. The calculated values of $\rho^{-2}\pi_t(k)$ are given in table 2 and plotted in figure 3. The constant of proportionality for the subrange of $\pi(k)$ has been obtained from the integration as $\alpha_p = 1.32\alpha^2$, so that

$$\frac{1}{\rho^2}\pi_t(k) = 1.32\alpha^2\epsilon^{\frac{4}{3}}k^{-\frac{7}{3}}. \tag{7.11}$$

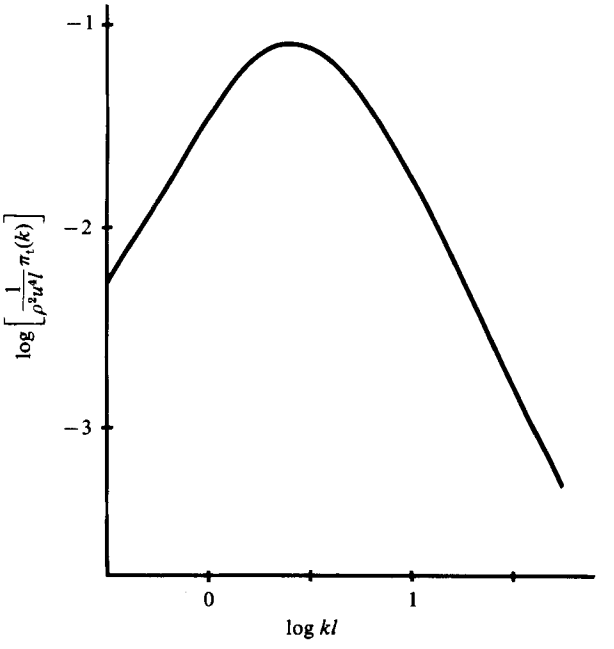

FIGURE 3. Turbulence–turbulence pressure-spectrum function.

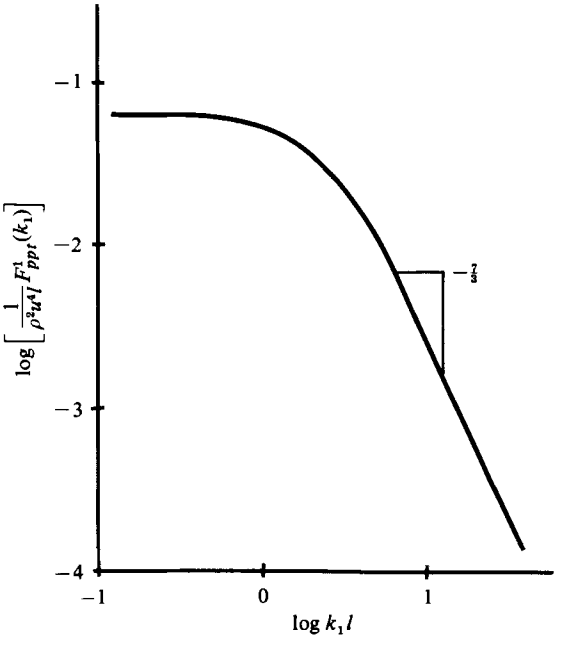

FIGURE 4. One-dimensional turbulence–turbulence pressure spectrum.

The coefficient is identical with that estimated from the pressure-fluctuation structure function by Monin & Yaglom (1975) using the results of Obukhov (1949).

The one-dimensional spectrum (which could be measured) can be calculated from the isotropic relation as

$$F^1_{ppt}(k_1) = \frac{1}{2}\int_{k_1}^{\infty} \frac{\pi_t(k)}{k}\,\mathrm{d}k. \tag{7.12}$$

The normalized results are summarized in table 2 and are plotted in figure 4. It follows from (7.12) that the one-dimensional version of the inertial subrange is†

$$F^1_{ppt}(k_1) = \tfrac{3}{14}(1.32)\,\epsilon^{\frac{4}{3}}\alpha^2 k_1^{-\frac{7}{3}}. \tag{7.13}$$

8. Higher-order velocity spectra and their relation to pressure spectra

An immediate consequence of isotropy is that the fourth-order velocity spectrum can be written as (cf. Monin & Yaglom 1975)

$$\begin{aligned}
F_{ij,\,mn}(\boldsymbol{k}) = {} & (F_{LL,\,LL} - 2F_{LL,\,NN} - 4F_{LN,\,LN} + F_{NN,\,NN})\frac{k_i k_j k_m k_n}{k^4} \\
& + (F_{LN,\,LN} - F_{NN,\,NN} + F_{NM,\,NM} + F_{NN,\,MM})\frac{k_j k_m \delta_{in} + k_i k_n \delta_{jm}}{k^2} \\
& + (F_{LL,\,NN} - F_{NN,\,MM})\frac{k_i k_j \delta_{mn} + k_m k_n \delta_{ij}}{k^2} \\
& + (F_{LN,\,LN} - F_{NM,\,NM})(k_i k_m \delta_{jn} + k_j k_n \delta_{im}) \\
& + (F_{NN,\,NN} - F_{NM,\,NM} - F_{NN,\,MM})\delta_{in}\delta_{jm} \\
& + F_{NM,\,NM}\delta_{im}\delta_{jn} + F_{NN,\,MM}\delta_{ij}\delta_{mn}.
\end{aligned} \tag{8.1}$$

The $F_{LL,\,LL}$, $F_{LL,\,NN}$, etc. are functions of k and are Fourier analogues of their more familiar counterparts, the correlation functions $B_{LL,\,LL}$, etc. The subscript L indicates that the Fourier velocity component is aligned with the wavenumber vector, while M and N indicate orthogonality.

Direct substitution of (8.1) into (7.1) yields

$$\frac{1}{\rho^2}F^t_{p,\,p}(\boldsymbol{k}) = F_{LL,\,LL}(k). \tag{8.2}$$

This equivalence of the pressure spectrum and one of the fourth-order velocity spectra is cause for some concern, since Van Atta & Wyngaard (1975) showed that the one-dimensional fourth-order velocity spectrum $F^1_{11,\,11}(k_1)$ has a $k_1^{-\frac{5}{3}}$ inertial subrange. This is especially worrisome, since they began with the same quasi-normal hypothesis relating fourth-order moments to second-order moments.

By noting that

$$\left.\begin{aligned}
F_{LL,\,LL} &= F_{11,\,11}(k,0,0), & F_{NN,\,NN} &= F_{22,\,22}(k,0,0), \\
F_{LL,\,NN} &= F_{11,\,22}(k,0,0), & F_{NM,\,NM} &= F_{23,\,23}(k,0,0), \\
F_{LN,\,LN} &= F_{12,\,12}(k,0,0), & F_{NN,\,MM} &= F_{22,\,33}(k,0,0),
\end{aligned}\right\} \tag{8.3}$$

† Note that this must be multiplied by 2 to obtain the corresponding half-line spectrum value.

kl	$F_{LL,LL}$	$F_{LL,NN}$	$F_{LN,LN}$	$F_{NN,NN}$	$F_{NN,MM}$	$F_{NM,NM}$
0.05623	1.61×10^{-4}	2.00×10^{-5}	7.03×10^{-5}	1.61×10^{-4}	2.01×10^{-5}	7.03×10^{-5}
0.1000	5.07×10^{-4}	6.28×10^{-5}	2.22×10^{-4}	5.07×10^{-4}	6.34×10^{-5}	2.22×10^{-4}
0.1778	1.59×10^{-3}	1.93×10^{-4}	7.00×10^{-4}	1.60×10^{-3}	1.99×10^{-4}	6.98×10^{-4}
0.3162	4.89×10^{-3}	5.61×10^{-4}	2.18×10^{-3}	4.97×10^{-3}	6.11×10^{-4}	2.18×10^{-3}
0.3981	7.55×10^{-3}	8.24×10^{-4}	3.41×10^{-3}	7.76×10^{-3}	9.44×10^{-4}	3.40×10^{-3}
0.5012	1.15×10^{-2}	1.16×10^{-3}	5.30×10^{-3}	1.21×10^{-2}	1.44×10^{-3}	5.31×10^{-3}
0.6310	1.73×10^{-2}	1.50×10^{-3}	8.13×10^{-3}	1.86×10^{-2}	2.16×10^{-3}	8.20×10^{-3}
0.7943	2.51×10^{-2}	1.68×10^{-3}	1.23×10^{-2}	2.84×10^{-2}	3.13×10^{-3}	1.26×10^{-2}
1.000	3.49×10^{-2}	1.37×10^{-3}	1.80×10^{-2}	4.29×10^{-2}	4.36×10^{-3}	1.93×10^{-2}
1.259	4.57×10^{-2}	7.981×10^{-5}	2.53×10^{-2}	6.40×10^{-2}	5.70×10^{-3}	2.91×10^{-2}
1.413	5.08×10^{-2}	-1.05×10^{-3}	2.93×10^{-2}	7.74×10^{-2}	6.35×10^{-3}	3.56×10^{-2}
1.585	5.53×10^{-2}	-2.50×10^{-3}	3.35×10^{-2}	9.29×10^{-2}	6.92×10^{-3}	4.31×10^{-2}
1.995	6.10×10^{-2}	-6.05×10^{-3}	4.11×10^{-2}	1.28×10^{-1}	7.62×10^{-3}	6.05×10^{-2}
2.512	6.07×10^{-2}	-9.46×10^{-3}	4.62×10^{-2}	1.63×10^{-1}	7.59×10^{-3}	7.76×10^{-2}
3.162	5.45×10^{-2}	-1.15×10^{-2}	4.74×10^{-2}	1.86×10^{-1}	6.81×10^{-3}	8.93×10^{-2}
3.981	4.46×10^{-2}	-1.15×10^{-2}	4.47×10^{-2}	1.89×10^{-1}	5.56×10^{-3}	9.18×10^{-2}
5.012	3.36×10^{-2}	-9.98×10^{-3}	3.91×10^{-2}	1.74×10^{-1}	4.20×10^{-3}	8.49×10^{-2}
6.310	2.37×10^{-2}	-7.78×10^{-3}	3.23×10^{-2}	1.47×10^{-1}	2.96×10^{-3}	7.23×10^{-2}
7.943	1.60×10^{-2}	-5.60×10^{-3}	2.55×10^{-2}	1.18×10^{-1}	2.00×10^{-3}	5.78×10^{-2}
10.000	1.04×10^{-2}	-3.81×10^{-3}	1.95×10^{-2}	8.95×10^{-2}	1.29×10^{-3}	4.42×10^{-2}
15.849	4.04×10^{-3}	-1.57×10^{-3}	1.06×10^{-2}	4.79×10^{-2}	5.05×10^{-4}	2.37×10^{-2}
31.623	8.85×10^{-4}	-3.59×10^{-4}	3.87×10^{-3}	1.68×10^{-2}	1.11×10^{-4}	8.36×10^{-3}
100.000	6.34×10^{-5}	-2.62×10^{-5}	6.37×10^{-4}	2.65×10^{-3}	7.91×10^{-6}	1.32×10^{-3}
316.228	4.37×10^{-6}	-1.83×10^{-6}	9.86×10^{-5}	4.00×10^{-4}	5.46×10^{-7}	2.0×10^{-4}
1000.000	2.98×10^{-7}	-1.23×10^{-7}	1.54×10^{-5}	5.53×10^{-5}	3.72×10^{-8}	2.77×10^{-5}

TABLE 3. Fourth-order velocity-spectrum functions

and again using the quasi-normal hypothesis, it is possible to obtain these spectral functions in integral forms analogous to (7.3)–(7.9). Again using the modified von Kármán spectrum for $E(k)$, each spectral function can be calculated. The results are summarized in table 3 and are plotted in figure 5.

It is immediately clear that the $k^{-\frac{7}{3}}$ range in the turbulent pressure spectrum and the $k^{-\frac{5}{3}}$ range in the fourth-order velocity spectra are consistent. The pressure spectrum depends only on $F_{LL,LL}$, which has a $k^{-\frac{7}{3}}$ inertial subrange, while the fourth-order velocity spectrum which depends on all of these is dominated by $F_{NN,NN}$, $F_{NM,NM}$ and $F_{LN,LN}$, which have $k^{-\frac{5}{3}}$ inertial subranges. An interesting feature of $F_{LL,NN}$ is that it is negative for high wavenumbers. The inertial-subrange constants obtained from the calculations are summarized in table 4.

A summation of all of the fourth-order velocity spectra of (8.1) has been carried out to obtain the one-dimensional fourth-order velocity spectrum $F^1_{11,11}(k_1)$. The results are indistinguishable from the analysis and experimental data of Van Atta & Wyngaard (1975). The agreement with the results and data of Van Atta & Wyngaard gives considerable confidence in the use of the quasi-normal hypothesis for the inertial-subrange calculations, and the semi-empirical form for $E(k)$ given by (6.9) and the deductions from it.

9. The net pressure spectrum

The net pressure spectrum is the sum of the contributions due to the turbulence–mean-shear interaction and the turbulence–turbulence interaction. Their relative contribution depends on the magnitude of the ratio Kl/u. Two cases will be illustrated

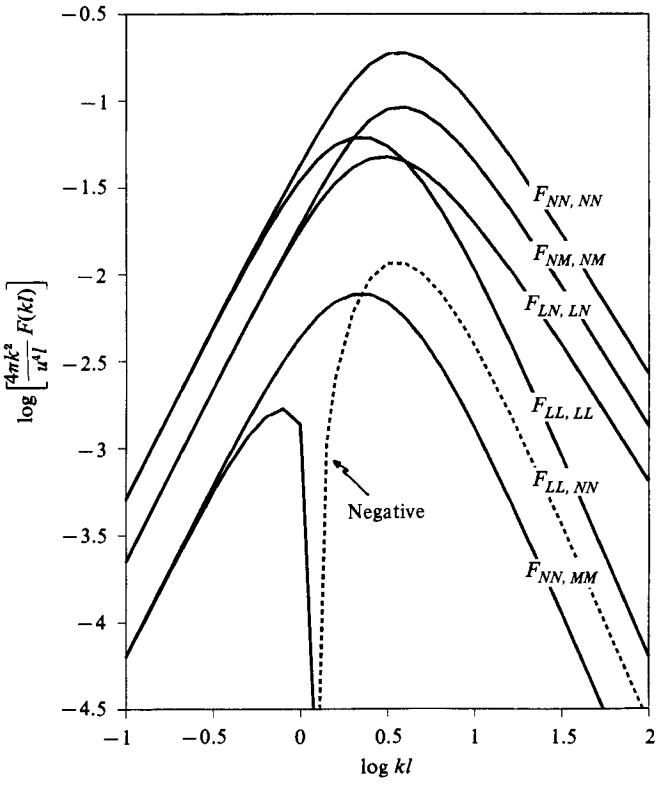

FIGURE 5. Fourth-order velocity-spectrum functions.

$\alpha^{-2}\epsilon^{-\frac{4}{3}}k^{\frac{7}{3}}(4\pi k^2 F_{LL,LL}) = 1.32$	$\alpha^{-2}\epsilon^{-\frac{4}{3}}k^{\frac{8}{3}}(4\pi k^2 F_{NN,NN}) = 5.77$
$\alpha^{-2}\epsilon^{-\frac{4}{3}}k^{\frac{7}{3}}(4\pi k^2 F_{LL,NN}) = -1.24$	$\alpha^{-2}\epsilon^{-\frac{4}{3}}k^{\frac{8}{3}}(4\pi k^2 F_{LN,LN}) = 1.60$
$\alpha^{-2}\epsilon^{-\frac{4}{3}}k^{\frac{7}{3}}(4\pi k^2 F_{NN,MM}) = 0.370$	$\alpha^{-2}\epsilon^{-\frac{4}{3}}k^{\frac{8}{3}}(4\pi k^2 F_{NM,NM}) = 2.86$

TABLE 4. Inertial-subrange constants for fourth-order velocity-spectrum functions

here: $Kl/u = 1$ and $Kl/u = 2.95$. The former represents a value typical of many shear flows, while the second is close to the maximum observed value and corresponds closely to the jet experiment described in Part 2 of this paper and to the atmospheric surface layer.

The one-dimensional spectra for $Kl/u = 2.95$ are shown in figure 6. As expected, the contribution of the mean-shear–turbulence interaction dominates at wavenumbers near the peak in turbulent energy, with the result that the net pressure spectrum also shows a pronounced peak. Note that, while there is evidence of the presence of the $k^{-\frac{11}{3}}$ region, its existence would not be at all obvious because of contributions in the same range from the turbulence–turbulence interaction. In fact, a $k^{-\frac{7}{3}}$ to $k^{-\frac{8}{3}}$ line could be drawn through the region to the right of the peak.

The one-dimensional spectra for $Kl/u = 1.0$ are shown in figure 7. Although the mean-shear–turbulence contribution is still present and contributes almost as much to the mean-square pressure fluctuations as does the turbulence–turbulence interaction

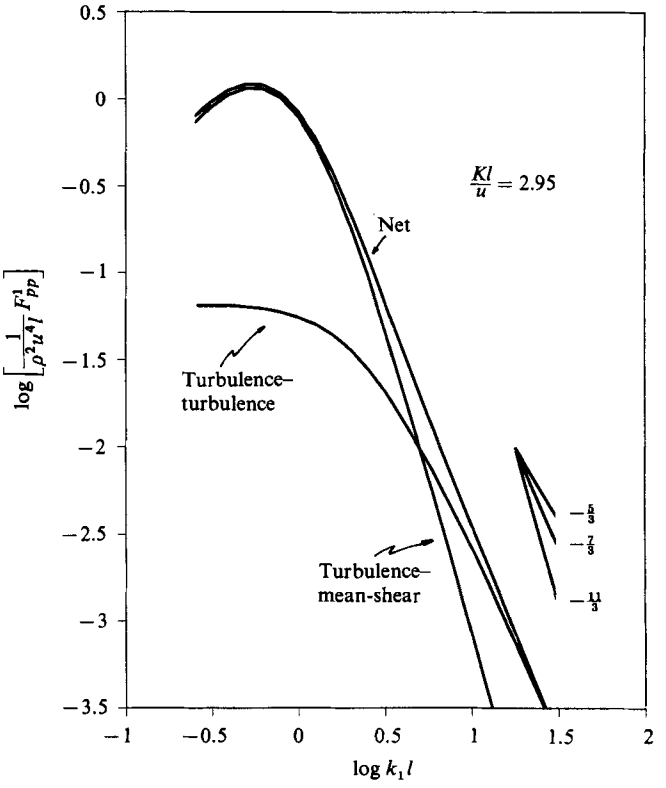

FIGURE 6. Net one-dimensional spectrum for $Kl/u = 2.95$.

(see §10), the $k^{-\frac{11}{3}}$ range is not present (except in the constituent spectrum) and only a small peak is observed. In fact, if a line is drawn using only the data between $kl = 1$ and 10, an experimenter could be led to believe that a $k^{-\frac{5}{3}}$ range was more appropriate, since the $k^{-\frac{7}{3}}$ range does not become apparent until after $kl = 10$.

It should be clear from these examples that the shear contribution will be impossible to isolate from spectral data, even in flows with moderate-to-high shear rates relative to the turbulence shear rate u/l. Therefore it is not surprising that such a range has not been previously observed. Moreover, in view of the limited frequency response of many probes and the multiplicity of results that are possible if only data below $kl = 10$ is used, it is not surprising that there is confusion in the literature regarding the existence of the $k^{-\frac{7}{3}}$ range.

10. The mean-square pressure fluctuation

The net pressure spectrum can be integrated to yield the mean-square turbulent pressure fluctuation

$$\overline{p^2} = \overline{p_s^2} + \overline{p_t^2}, \tag{10.1}$$

where

$$\overline{p_s^2} = \int_0^\infty \pi_s(k)\,\mathrm{d}k \tag{10.2}$$

and

$$\overline{p_t^2} = \int_0^\infty \pi_t(k)\,\mathrm{d}k. \tag{10.3}$$

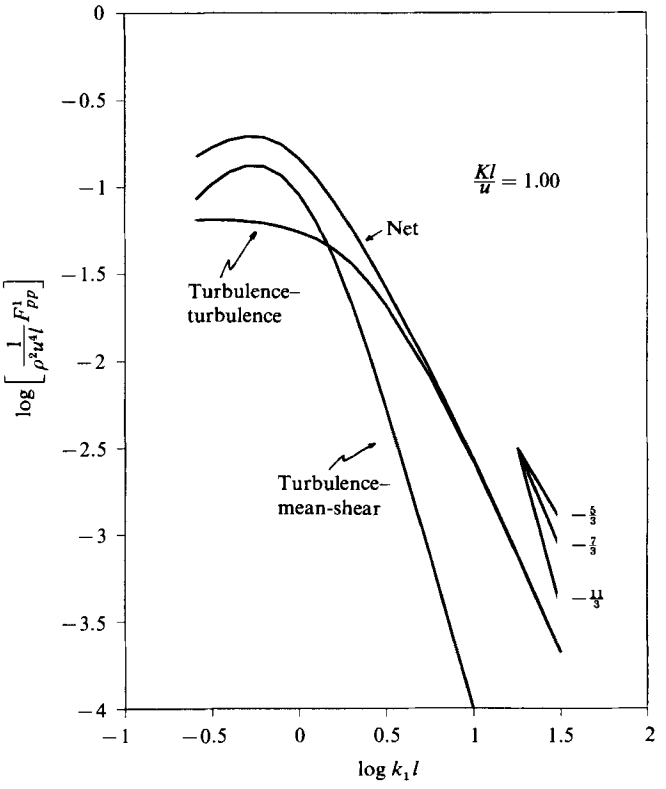

FIGURE 7. Net one-dimensional spectrum for $Kl/u = 1.0$.

Direct integration of the turbulence–mean-shear interaction spectrum of (6.5) and (6.9) yields

$$\frac{1}{\rho^2}\overline{p_s^2} = 0.33K^2l^2u^2, \tag{10.4}$$

where l is the lengthscale defined by (6.13) and u is the velocity scale defined by (6.10). This can be compared with the results of Kraichnan (1956) cited in (1.1). The exact value of the coefficient is dependent on the particular spectral model used. In view of the fact that the spectrum peaks sharply at low wavenumbers, where its shape depends strongly on flow geometry, any applicability of this result to a real shear flow should be regarded as fortuitous. However, for flows characterized by single time- and lengthscales (Kl/u = const), the result must be dimensionally correct, although the coefficient depends on the flow geometry.

The turbulence–turbulence spectrum can be integrated numerically to yield

$$\overline{p_t^2} = 0.42\rho^2u^4. \tag{10.5}$$

This is close to results of Hinze (1959) and Uberoi (1953), who obtained a coefficient of 0.49, but is somewhat higher than Batchelor's estimate of 0.34. The agreement with Uberoi's result is especially significant, since unlike the others he used the measured fourth-order velocity correlations to calculate the mean-square turbulent pressure fluctuations.

In summary, the mean-square turbulent pressure fluctuations for homogeneous turbulent flow superimposed on an uniform mean shear have been calculated as

$$\frac{1}{\rho^2}\overline{p^2} = 0.33K^2l^2u^2 + 0.42u^4, \tag{10.6}$$

where the first coefficient depends on the spectral model used. Note that we can be more optimistic about the applicability of spectral models at wavenumbers above that corresponding to the peak (because of local isotropy) than about the mean-square values which are strongly influenced by the large-scale anisotropic fluctuations.

11. The mean-square pressure-gradient fluctuation

The mean-square fluctuating pressure gradient is given by

$$\overline{(\nabla p)^2} = \int_0^\infty k^2 \pi(k)\,\mathrm{d}k. \tag{11.1}$$

As pointed out by Heisenberg (1948) and Batchelor (1951), the pressure-gradient fluctuations will be dominated by wavenumbers in the inertial subrange since, unlike the velocity spectrum, the pressure spectrum falls more rapidly than k^{-2}.

The contribution of the mean-shear–turbulence interaction can be obtained directly using (6.5), with the result that

$$\overline{(\nabla p)_{\mathrm{s}}^2} = \int_0^\infty k^2 \pi_{\mathrm{s}}(k)\,\mathrm{d}k = \tfrac{8}{5}\rho^2K^2u^2, \tag{11.2}$$

where we have used the fact that the integral of $E(k)$ is $\frac{3}{2}u^2$.

The turbulence–turbulence contribution to the mean-square pressure-gradient fluctuation cannot be obtained by directly integrating $k^2\pi_{\mathrm{t}}$ using the previously obtained values of π_{t}. This is because $k^2\pi_{\mathrm{t}} \to k^{-\frac{1}{3}}$ for large wavenumbers, and therefore cannot be integrated over an infinite domain. Thus, as noted by Batchelor, the value of $\overline{(\nabla p)_{\mathrm{t}}^2}/\rho^2$ will depend on the extent of the equilibrium range and in turn is dependent on the turbulent Reynolds number ul/ν (or alternatively l/η).

George (1974) and Jones *et al.* (1979) showed that the pressure spectrum in Kolmogorov variables could be written as

$$\frac{1}{\rho^2}\pi_{\mathrm{t}}(k) = \epsilon^{\frac{3}{4}}\nu^{\frac{7}{4}} f_{\mathrm{t}}(k\eta) \tag{11.3}$$

and that the $k^{-\frac{7}{3}}$ range could be obtained by an asymptotic matching of the function f_{t} with the analogous low-wavenumber function F_{t} given by

$$\frac{1}{\rho^2}\pi_{\mathrm{t}}(k) = u^4 l\, F_{\mathrm{t}}(kl) \tag{11.4}$$

in the limit as $l/\eta \to \infty$. We can use these to write

$$\frac{1}{\rho^2}\overline{(\nabla p)_{\mathrm{t}}^2} = u^4 l^{-2}\left(\int_0^{Al/\eta} \mathrm{d}(kl)\,(kl)^2\, F_{\mathrm{t}}(kl) + R_l^{-1}\int_A^\infty \mathrm{d}(k\eta)\,(k\eta)^2 f_{\mathrm{t}}(k\eta)\right), \tag{11.5}$$

where A is a constant and is determined so that the integral is divided in the inertial subrange (the $k^{-\frac{7}{3}}$ range) where both scaling laws are valid.

The second integral can be ignored in the limit of large R_l, since the integral is an

absolute constant. The first integral can be further subdivided if Al/η is large enough (say greater than 30) so that

$$\int_0^{Al/\eta} \mathrm{d}kl \ldots = \int_0^{30} \mathrm{d}kl \ldots + \int_{30}^{Al/\eta} \mathrm{d}kl \ldots . \tag{11.6}$$

Since by $kl = 30$ the inertial-subrange formula is approximately valid, the second integral can be obtained analytically, while the first can be obtained by numerically integrating $k^2\pi_t$. Thus for $Al/\eta > 30$ the following relationship is approximately valid:

$$\frac{1}{\rho^2}\overline{(\nabla p)_t^2} \approx u^4 l^{-2}\left[4.61\left(A\frac{l}{\eta}\right)^{\frac{2}{3}} - 16.94\right]. \tag{11.7}$$

If A is chosen as 0.15 to correspond to the peak in the dissipation spectrum (where the energy spectrum starts to roll off rapidly), this expression can be further reduced to

$$\frac{1}{\rho^2}\overline{(\nabla p)_t^2} \approx u^4 l^{-2}[1.30R_l^{\frac{1}{2}} - 16.94] \tag{11.8}$$

for $R_l > 2000$.

Batchelor (1951) cites the approximate relation

$$\frac{1}{\rho^2}\overline{(\nabla p)_t^2} = 226\nu\frac{u^3}{\lambda^3}. \tag{11.9}$$

Using $R_\lambda = \sqrt{30}\, R_l^{\frac{1}{2}}$, (11.8) can be rewritten as

$$\frac{1}{\rho^2}\overline{(\nabla p)_t^2} \approx 214\nu\frac{u^3}{\lambda^3}\left[1 - \frac{16.94}{R_\lambda}\right], \tag{11.10}$$

which is very close to Batchelor's result as $R_\lambda \to \infty$. The slight difference in these results arises from the manner in which the spectral truncation is carried out in (11.5).

Part 2. Measurement and comparison with theory

12. Relevance of theory to jet-mixing-layer experiment

In Part 2 of this paper our objective is to present experimental data against which the theoretical considerations of Part 1 can be tested. Because of the limitations imposed by the assumption of isotropy (at all wavenumbers), quantitative comparisons should be possible only at wavenumbers corresponding to the inertial subrange (assuming the Reynolds number is high enough), where local isotropy can reasonably be assumed. However, in view of the frequent success of isotropic theories beyond the expected range of validity, one might reasonably expect at least qualitative agreement at much lower wavenumbers than those for which isotropy can be assumed. We shall see that this is indeed the case for the jet-mixing-layer experiment reported here.

The measurements presented below were taken at the centre of the mixing layer of an axisymmetric turbulent jet. This particular flow has the advantage of a relatively high turbulence intensity, which helps raise the pressure signal produced above that of the background noise. In addition the ratio of the mean shear rate K to the turbulence scale u/l is about the largest value which can be obtained in a laboratory flow, thus maximizing the importance of the turbulence–mean-shear-rate contribution relative to that of the turbulence–turbulence interaction. Finally, the fact that the mixing layer grows in approximately similar fashion provides a

convenient way to scale the data, an advantage if a range of scales is desired and if non-scaling measurement errors are suspected. The jet mixing layer does have the disadvantage that the turbulence is strongly inhomogeneous in the radial direction. Even so, as Davies, Fischer & Barrett (1963) and Bradshaw, Ferris & Johnson (1964) have shown, the integral scales are nearly independent of radius, and the inhomogeneity is almost entirely due to intermittency.

In the following sections we shall first review previous attempts to measure fluctuating pressures. Then we analyse the response of any pressure probe to velocity contamination and discuss the particular characteristics of our probe. The problems of interpreting spectral measurements in high-intensity flows are briefly reviewed because of the increasingly important role these effects play as the rate of spectral roll-off increases. The basic characteristics of our jet are discussed and spectral data for the fluctuating pressures are presented. Finally the data are compared with the theory of Part 1.

13. Historical background of attempts to measure pressure fluctuations

The first serious attempts to measure fluctuating pressures in free turbulent flow appear to be due to Rouse (1953), Kobashi (1957) and Kobashi, Kono & Nishi (1960). Rouse measured in turbulent cylinder wakes. Attempts to extend the work of Rouse were made by Sami, Carmody & Rouse (1967) and Igarishi & Fujisama (1968). Further attempts at cylinder-wake measurements were made by Strasberg (1963) and Mackawa (1965).

An intensive study of the pressure fluctuations in an axisymmetric jet mixing at UTIAS was reported by Siddon (1969), who constructed a special probe to compensate for velocity contamination. Encouraged by Siddon's success, numerous investigators began to measure jet-pressure fluctuations with a variety of techniques. Jones and his coworkers at the University of Illinois developed a helium-bleeder probe for jet-mixing-layer measurements (Spencer 1974; Spencer & Jones 1971; Planchon 1974). Arndt and his coworkers at the Pennsylvania State University developed a probe similar to Siddon's without compensation and reported mixing-layer fluctuating-pressure measurements (Arndt & Nilsen 1971; Arndt, Tran & Barefoot 1974); this probe will be discussed in detail later. Fuchs and coworkers at the Institute for Turbulence Research, DFVLR, Berlin, reported extensive measurements using shrouded microphones (Fuchs 1970, 1972; Michalke & Fuchs 1975). Later in this paper it will be shown that the measurements taken by all of these groups using four different techniques produce the same spectra for the jet mixing layer and that these measurements are in agreement with the theoretical spectrum predicted earlier in this paper.

Elliot (1972) used a probe based on a fluctuating-lift principle to measure pressure spectra in the atmosphere. Application of the criteria developed in this section suggest that his measurements are in error, at least at the highest frequencies, since they yielded spectra unlike the expected pressure spectra but very much like the spectrum expected where velocity-contamination effects dominate. On the other hand, recent measurements by Mikkelsen (1978), using a probe similar to that used by Miksad (1976) in the atmospheric boundary layer, as well as the earlier measurements of Gossard (1960), satisfy the criteria proposed here and appear to be relatively uninfluenced by velocity fluctuations.

Numerous attempts have been made in the past twenty years to measure the wall-pressure fluctuations beneath a turbulent flow (for a summary see Willmarth

1975). These measurements are not of interest here, since we have confined our attention to turbulent free shear flow at high turbulence Reynolds number in the absence of boundary effects.

14. The measurement of turbulent pressure fluctuations

The effect of flow–probe interactions on attempts to measure static-pressure fluctuations with Pitot–static-type probes has been investigated in detail by Siddon (1969) and Fuchs (1972). Fuchs lists the following possible sources of measurement error:

(i) *acoustic contamination* due to spurious disturbances superimposed on the flow and originating exterior to it;

(ii) *wind noise* arising from the flow over the aerodynamic body containing the pressure-sensitive orifice;

(iii) *acceleration response* to flow-induced vibrations of the probe;

(iv) *flow-affected sensitivity* arising from, for example, directional effects;

(v) *resolution error* due to averaging over the surface of the probe;

(vi) *error due to fluctuating cross-flow*;

(vii) *response to axial-velocity fluctuations.*

In the tests by Fuchs and Siddon and in those of the present investigation, the sources (i)–(iv) could be shown not to be significant contributors to pressure-measurement error by a variety of experiments in turbulent and non-turbulent flow. These experiments have been described in detail by Fuchs (1972), Siddon (1969) and Arndt & Nilsen (1971).

The problem of spatial averaging by finite probes (v) is one of the classical problems of turbulence measurement. While corrections could be derived for the averaging of disturbances over the finite sensing area of the probe, the safest approach (and that utilized in this investigation) is to regard as unreliable any measurement corresponding to scales smaller than twice the size of the probe. For the Pitot–static probe introduced in §15 (shown schematically in figure 8) we estimate this 'size' to be the distance of the sensing holes from the tip of the tube, or five probe diameters ($5 \times \frac{1}{8}$ in.).

The errors arising from the axial and cross-flow fluctuations were investigated both theoretically and experimentally by Siddon (1969) and Fuchs (1972). Siddon, following the earlier work of Strasberg (1963), postulated that the error at a given scale of measurement depended only on the local instantaneous velocity and its derivatives; that is,

$$\frac{1}{\rho}[\tilde{p}_{\mathrm{m}}(t)-\tilde{p}(t)] = f\left\{\tilde{u}, \tilde{v}, \tilde{w}, \frac{\partial \tilde{u}}{\partial t}, \frac{\partial \tilde{v}}{\partial t}, \frac{\partial \tilde{w}}{\partial t}\right\}, \tag{14.1}$$

where $\tilde{p}_{\mathrm{m}}(t)$ is the measured instantaneous static pressure and $\tilde{p}(t)$ is the value it would have had were the probe not there.

By expanding (14.1) for small values of the arguments, insisting on an error that is invariant to reflections about the probe axis (since the probe cannot distinguish between positive and negative cross-flow), and neglecting the acceleration terms, Siddon obtained an expression for the error (in isotropic flow) as

$$\frac{1}{\rho}[\tilde{p}_{\mathrm{m}}(t)-\tilde{p}(t)] = A\tilde{u}^2(t)+B[\tilde{v}^2(t)+\tilde{w}^2(t)]. \tag{14.2}$$

By decomposing into mean and fluctuating parts, the error in mean static-pressure measurement can be obtained as

$$\frac{1}{\rho}[P_m - P] = A(U^2 + \overline{u^2}) + B(\overline{v^2} + \overline{w^2}), \tag{14.3}$$

while the error in the fluctuating pressure is

$$\frac{1}{\rho}[p_m - p] = A[2Uu + (u^2 - \overline{u^2})] + B[(v^2 - \overline{v^2}) + (w^2 - \overline{w^2})]. \tag{14.4}$$

It has been assumed that the probe is aligned with the flow so that the only non-zero component of mean velocity is the axial one. The coefficient A measures the sensitivity to streamwise velocity fluctuations, while B measures the sensitivity to cross-flow disturbances.

Fuchs (1972) arrived at a similar result for the effect of the streamwise disturbances (the first term in the equations above) from the unsteady streamline Bernoulli equation. He was also able to show directly that the neglect of the acceleration terms was justified as long as the diameter of the probe was significantly less than the scale of the pressure disturbance. This condition has already been imposed here by the spatial-resolution criterion adopted earlier.

Siddon and Fuchs noted that the sensitivity to streamwise velocity variations could be minimized by proper positioning of the sensitive ports. For Siddon's probe (and the probe used here) $A \approx 0$, while Fuchs estimated $A \approx -0.075$ for his shrouded microphone. Siddon estimated the upper bound on the cross-flow error to be $B \approx -0.45$, and designed a special probe to compensate for this. His measurements indicated that B seems to depend on the turbulence parameters, at least in the jet mixing layer. For measurements along the centre of the mixing layer in an axisymmetric jet ($r = \frac{1}{2}D$), Siddon found less than 1 dB difference between spectra measured with his compensated and uncompensated probes. We shall see later that this implies that $|B|$ must be substantially less than 0.45 in the mixing-layer centre.

The error in the mean-square static-pressure fluctuation is readily obtained from (14.4) as

$$\begin{aligned}
&\frac{1}{\rho^2}[\overline{p_m^2} - \overline{p^2}] \\
&= \left(A\left[\frac{2}{\rho}U\overline{pu} + \overline{pu^2}\right] + B[\overline{pv^2} + \overline{pw^2}]\right) \\
&\quad + (A^2[4U^2\overline{u^2} + 4U\overline{u^3} + \overline{(u^2 - \overline{u^2})^2}] + AB[2U(\overline{uv^2} + \overline{uw^2}) + \overline{(u^2 - \overline{u^2})(v^2 - \overline{v^2})} \\
&\quad + \overline{(u^2 - \overline{u^2})(w^2 - \overline{w^2})}] + B^2[\overline{(v^2 - \overline{v^2})^2} + \overline{(v^2 - \overline{v^2})(w^2 - \overline{w^2})} + \overline{(w^2 - \overline{w^2})^2}]).
\end{aligned} \tag{14.5}$$

Since our interest here is only in the universal-equilibrium range of the turbulence spectrum, we will assume isotropy. Moreover, we shall neglect third-order moments of the velocity. Immediate consequences of these assumptions on (14.5) are the elimination of the $\overline{pu}$ correlation as well as $\overline{uv^2}$, $\overline{uw^2}$ and $\overline{u^3}$. The spectral decomposition of this reduced equation is readily shown to be

$$\begin{aligned}
\frac{1}{\rho^2}[F_m - F_{p,p}] = \frac{1}{\rho}(AF_{p,11} + B[F_{p,22} + F_{p,33}]) + (A^2[4U^2F_{1,1} + F_{11,11}] \\
+ AB[F_{11,22} + F_{11,33}] + B^2[F_{22,22} + F_{22,33} + F_{33,33}]),
\end{aligned} \tag{14.6}$$

where the Fs are the three-dimensional spectra and the argument $\boldsymbol{k}$ is suppressed for convenience.

Equation (14.6) can be further decomposed into spectra involving only velocities by noting that isotropy implies (cf. Monin & Yaglom 1975)

$$F_{p,ij} = \frac{F_{p,LL} - F_{p,NN}}{k^2} k_i k_j + F_{p,NN}\,\delta_{ij} \tag{14.7}$$

and

$$F_{p,LL} = -\rho F_{LL,LL}, \qquad F_{p,NN} = -\rho F_{LL,NN}. \tag{14.8), (14.9}$$

By direct substitution, the error spectrum of (14.6) can be derived in terms of our previously derived velocity spectral functions. Reference to figure 5 indicates that the errors arising from the pressure–velocity-squared correlations will present the most serious problem since they have the same $k^{-\frac{7}{3}}$ slope as the pressure. All of the other terms will have an easily recognizable $k^{-\frac{5}{3}}$ slope, which will dominate the pressure spectrum, if significant.

By applying the results of §8 to (14.6)–(14.9), integrating over k_2 and k_3 to get the one-dimensional spectra, and dividing by F^1_{ppt}, the relative error in the measured one-dimensional pressure spectrum in the inertial subrange can be shown to be given by

$$\frac{[F^1_m(k_1) - F^1_{p,p}(k_1)]}{F^1_{p,p}(k_1)} \approx [-0.6A - 0.9B - 0.4AB - 0.26B^2] + \left[1.6A^2\left(1 + \frac{U^2}{u^2}\right) + 4.4B^2\right](kl)^{\frac{2}{3}}. \tag{14.10}$$

The first term represents the contribution from the pressure–velocity-squared correlations ($k^{-\frac{7}{3}}$ error), while the second represents the leading axial and cross-flow contributions ($k^{-\frac{5}{3}}$ error). It is interesting to note that the effect of the axial-velocity fluctuations increases as the turbulence intensity decreases. This is because the pressure spectrum (denominator) decreases as u^4, while the velocity spectrum decreases only as u^2.

If the worst-case values of $A \sim -0.0075$ and $B \sim -0.45$ are used in (14.10) and we take $u/U \sim 0.25$ (which corresponds to the jet experiment described later), the $(kl)^{\frac{2}{3}}$ term dominates for $kl > 0.3$ and the relative error is unity near $kl \approx 0.6$. Since this is well below the wavenumber at which we expect the turbulence–turbulence contribution to become important, a $k^{-\frac{7}{3}}$ range will not be visible in the measured spectrum if the estimates of A and B are reasonable. For the probe used in the experiments described later, values of $A = -0.0075$ and $B = -0.15$ give a relative spectral error equal to unity at $kl \approx 26$, which is near that which is observed for the measurements in figures 14 and 15.

15. The static-pressure probe

The unsteady pressure probe used in this investigation was developed by Arndt & Nilsen (1969) and is shown in figure 8. The sensitive element is a Bruel & Kjaer $\frac{1}{8}$ in. condenser microphone, which is connected to a cathode follower and powered by a B & K Type 2801 Microphone Power Supply Unit. The probe is a standard Pitot–static tube, 0.125 in. outside diameter and 2.5 in. in length. Four static-pressure holes are spaced 90° apart and are located at a distance of 5 tube diameters from the tip of the probe to minimize sensitivity to cross-flow error. The leeward end of the probe is terminated by the microphone.

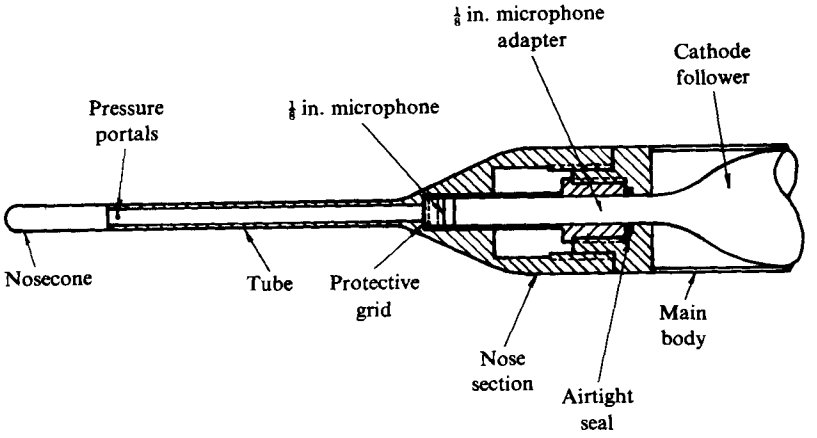

FIGURE 8. Schematic of pressure probe.

Several criteria were considered in selecting this probe design. These included the constraints that the components be off-the-shelf items in order to minimize development time and that the frequency response be as high as possible while minimizing probe size. The length of the tube was selected to minimize interference effects from the shroud while not compromising the frequency response. The frequency response of the system is limited by the Helmholtz-resonator response of the tube and microphone cavity and can be calculated from

$$\omega_c = \frac{a_0}{l_T}\left(\frac{\pi r_T^2 l_T}{V}\right), \tag{15.1}$$

(Strasberg 1963), where ω_c is the resonant frequency, V is the cavity volume, l_T is the length of tube, a_0 is the speed of sound and r_T is the tube radius. The resonant frequency f_c was computed to be 1000 Hz. In order to obtain a flat response over the broadest range of frequencies, damping material was placed in the probe tube to diminish a response peak at the tube resonant frequency. By trial and error, the damping was adjusted to be approximately 70 % of critical. (This value was estimated initially from the transient response of the device to impulsive pressures created by bursting balloons and verified during the calibration procedure when the steady-state response function was measured.) The frequency-response function under these conditions is given by

$$T(f) = \frac{1}{(1+(f/f_c)^4)^{\frac{1}{2}}}. \tag{15.2}$$

At the critical frequency the theoretical response is down by less than 0.2 dB. The phase lag induced by damping is quite large at frequencies approaching f_c, but this is not a factor in measuring spectra.

The response of the B & K cathode follower rolled off at frequencies less than 100 Hz, and a compensating network was developed to ensure an overall flat response of the probe to frequencies as low as 20 Hz. Thus the probe was designed to have flat response in the frequency range 20–1000 Hz. The upper limit is compatible with the frequency corresponding to the assumed spatial resolution given by

$$f_s = \frac{U_c}{10d}, \tag{15.3}$$

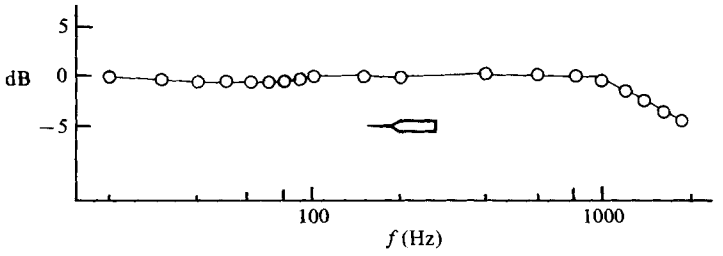

FIGURE 9. Probe frequency-response function.

where U_c is the convection velocity and d is the probe diameter. This corresponds to 700 Hz at a jet velocity of 30 m/s ($U_c \approx 18$ m/s).

The probe was calibrated in a small reverberant chamber using a 6 mm diameter B & K microphone as standard. Details of the calibration procedure are given in Arndt & Nilsen (1971). The measured frequency response is shown in figure 9. Sensitivity to angle of attack, determined by tests in uniform flow, indicated that the pressure measurements were insensitive to angles as high as 15°, corresponding to an equivalent turbulence level of 27 % (Barefoot 1972). Various other techniques used to determine the sensitivity to turbulence are described in Arndt & Nilsen (1971) and Bahnk (1971).

Probe alignment in the mean-flow direction was accomplished by using a special probe consisting of four hypodermic needles with their tips bevelled at 45° to the probe axis. By balancing the pressure sensed in each of two probes, alignment in two perpendicular planes was possible.

Acoustic contamination of the pressure signal from fan noise and other extraneous noise sources was also studied. Details are given in Barefoot (1972), who found that the optimum signal-to-noise ratio was obtained at a jet velocity of approximately 25 m/s. The variation in signal-to-noise ratio was only weakly dependent on velocity near the minimum; with fan noise as the major contributor at higher velocities, and extraneous sources of sound at lower velocities.

16. Taylor's hypothesis and spectral analysis

Taylor's hypothesis in its simplest form states that time variations seen by a fixed probe in a moving fluid are the result of spatially varying disturbances which are convected past the probe. This can, of course, never be strictly true for turbulence, since flow disturbances are both time- and space-dependent. In many cases, however, the temporal variations occur over times long compared with the time for disturbances to traverse the probe, and the temporally varying signal can be interpreted as a spatially varying one using

$$\frac{\partial}{\partial x} \approx \frac{1}{U_c}\frac{\partial}{\partial t}, \tag{16.1}$$

or the Fourier-transformed counterpart

$$k \approx \frac{2\pi f}{U_c}. \tag{16.2}$$

If the turbulence intensity is sufficiently great, Taylor's hypothesis in the form of (16.1) is not valid because of the fluctuating convection velocity. This is because a

single wavenumber can be mapped into a band of frequencies corresponding to the range of velocities which can convect it. The result is an aliasing (or spectral leakage) of the more energetic disturbances into adjacent wavenumbers which have less energy, thereby modifying the spectral shape. In general, the faster the roll-off (or rise) of the spectrum, the more serious the effect.

Lumley (1965) was able to derive a differential equation relating the spectrum inferred from (16.1) to the true streamwise velocity spectrum. Wyngaard & Clifford (1975) extended Lumley's analysis to include the cross-stream velocity spectra and scalar spectra. These equations assume that the convected field is isotropic. The equations are

streamwise velocity

$$F^{\mathrm{m}} = F + \frac{\overline{u_1^2}}{2U^2}\left((k^2F'' - 2F) - 2(kF' + F)\left[\frac{\overline{u_2^2} + \overline{u_3^2}}{\overline{u_1^2}} - 2\right]\right), \tag{16.3}$$

scalar

$$F^{\mathrm{m}} = F + \frac{\overline{u_1^2}}{2U^2}\left((k^2F'' + 2kF') - (2kF' + F)\left[\frac{\overline{u_2^2} + \overline{u_3^2}}{\overline{u_1^2}} - 2\right]\right), \tag{16.4}$$

where F^{m} denotes the measured spectrum, and in (16.3) and (16.4) F denotes the true one-dimensional streamwise velocity spectrum and the true scalar spectrum respectively.

It is easy to show by substitution that, if the spectrum has a power-law behaviour (as in the inertial subrange), the power law is unchanged but the coefficient is increased by an amount which depends on the turbulence intensity and the rate of roll-off; thus the measured spectrum overestimates the true spectrum. The overestimates for the spectra measured in §17 are 5% for the $k^{-\frac{5}{3}}$ range in the velocity spectra, and 8% and 28% for the $k^{-\frac{7}{3}}$ or $k^{-\frac{11}{3}}$ range in the pressure spectra. It follows that the dissipation will also be overestimated. In the jet mixing layer of §17 this overestimate is approximately 8%.

In a turbulent shear flow an additional problem can arise because disturbances at different wavenumbers can be convected at different velocities depending on their location in the flow. Lumley has established criteria for which the effect of spatial gradients on the convection velocity and the effects of the temporal evolution can be neglected and the disturbance can be assumed to be sweeping past the probe with the local instantaneous fluid velocity. In many turbulent shear flows (such as the jet mixing layer) these criteria are satisfied for disturbances at scales corresponding to the inertial subrange and smaller. They are not satisfied in the lower spectral range of interest in this experiment, and an approach given by Wills (1964) will be applied.

Wills suggests defining a wavenumber-dependent convection velocity that is valid at the larger scales where the equations above are not applicable. From measurements of the wavenumber–frequency cross-spectrum obtained from two-point velocity data, Wills substitutes kU_k for the frequency and seeks the wavenumber-dependent convection velocity that maximizes the value of the spectrum at fixed k, i.e.

$$\frac{\mathrm{d}}{\mathrm{d}U_k} F_{1,1}(k, kU_k) = 0. \tag{16.5}$$

The technique was applied to measurements taken in the mixing layer of an axisymmetric jet similar to the one described in §17. While measurements were taken at the centre of the mixing layer at only one axial position, since the flow is nearly

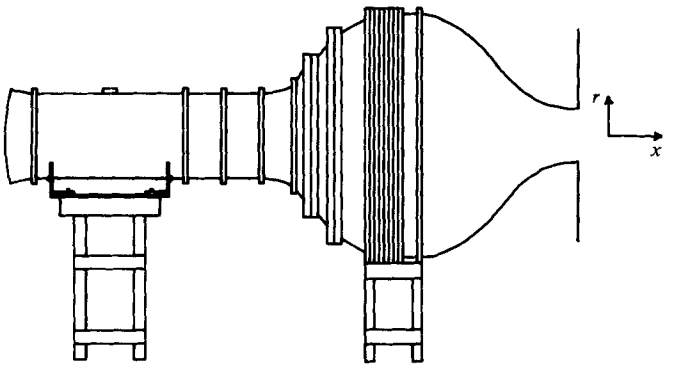

FIGURE 10. Schematic of the axisymmetric jet.

self-similar the results can be fitted with an empirical expression and scaled to yield for a limited range of wavenumbers

$$\frac{U_k}{U} = 0.57 + 0.013(kx)^{\frac{1}{2}} \quad (3 < kx < 300). \tag{16.6}$$

Wills also showed that the convection velocity averaged over all wavenumbers was nearly equal to the local mean velocity in the mixing layer. Equation (16.6) will be used in §18 for the pressure data.

17. The experimental facility and turbulence measurements

Experiments were carried out in the mixing layer of a 12 in. axisymmetric jet (shown schematically in figure 10). The flow characteristics of the mixing layer were investigated in detail by Von Frank (1970), Arndt *et al.* (1974) and Lauchle & George (1972). The profiles of the mean and r.m.s. fluctuating streamwise velocity are shown in figure 11. Although the dynamical equations do not admit similarity solutions, the data collapsed to the curves shown to within experimental error over the range $1 < x/D < 5$ when normalized by the jet velocity U_E and the distance x from the exit plane. Note that no virtual origin was required. (We believe this to be due to the fact that the contraction boundary layer is laminar at the exit plane and that its thickness is several orders of magnitude less than the diameter of the jet exit.)

Of particular interest in scaling the spectral data that will be presented is the rate of dissipation of turbulent energy ϵ. This cannot be directly measured because of the high turbulence Reynolds number and the resulting small Kolmogorov microscale; therefore it must be obtained indirectly. At high turbulence Reynolds number, the fact that the energy dissipation is controlled by the energy-containing scales of motion implies $\epsilon \sim u^3/l$, where $u^2 = \overline{u_1^2} + \overline{u_2^2} + \overline{u_3^2}$ and l is a lengthscale characteristic of these motions. Arndt *et al.* (1974), Davies *et al.* (1963) and Bradshaw *et al.* (1964) have shown that both mean-flow and turbulent correlations are nearly self-similar when scaled by x and U_E. Thus we have

$$\frac{u}{U_E} = \text{const}, \quad \frac{l}{x} = \text{const}, \quad \frac{\epsilon x}{U_E^3} = \text{const}, \tag{17.1}$$

where two of the constants must be chosen from the data. Direct measurements of $\overline{u_1^2}$, $\overline{u_2^2}$ and $\overline{u_3^2}$ indicate that $u/U_e \approx 0.16$.

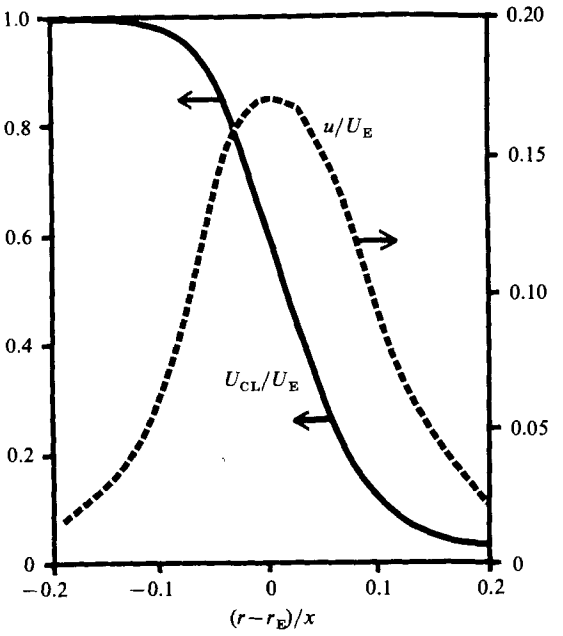

FIGURE 11. Profiles of mean and r.m.s. axial velocities in jet mixing layer normalized by similarity-like variables ($1 \leqslant x/D \leqslant 5$).

Figure 12 shows $F_{11}^1(k_1)_1$, the one-dimensional velocity spectrum, measured in a similar axisymmetric jet mixing layer by Khwaja (1980). Data were taken on the line for which $U = 0.6U_E$, which corresponds to an axial traverse from the jet lip. These spectra are nearly identical with those obtained in the facility used in the pressure experiments. The wavenumbers were computed from the measured frequency spectrum by assuming the flow to be frozen in space and swept by the probe with velocity $U_c = 0.6U_E$. This value corresponds to the convection velocity determined by Davies *et al.* (1963) from space–time correlation measurements and to the average convection velocity determined by Wills (1964) from the space–time cross-spectra. No corrections for the fluctuating convection velocity were applied to the data shown, but they were applied to the dissipation estimate below.

The spectra are seen to collapse, as expected, for wavenumbers through the inertial subrange when plotted as $F_{11}^1/U_E^2 x$ versus $k_1 x$, where k_1 is computed from Taylor's hypothesis as $k_1 = 2\pi f/U_c$. The inertial subrange ($k^{-\frac{5}{3}}$ range) corresponds to

$$\frac{F_{11}^1(k_1 x)}{U_E^2 x} = \tfrac{9}{55}\alpha(0.13)(k_1 x)^{-\frac{5}{3}}, \tag{17.2}$$

where $\alpha = 1.5$. It follows immediately from the Kolmogorov result that the measured dissipation ϵ_m is given by

$$\epsilon_m = 0.048\frac{U_E^3}{x}. \tag{17.3}$$

The spectrum and dissipation rate can be corrected for the spectral aliasing arising from the fluctuating convection velocity. From Lumley's result (16.3), the spectrum is too high in the inertial subrange by approximately 5%, and ϵ_m overestimates the true dissipation rate by almost 8%. Thus we obtain

$$\epsilon = 0.044U_E^3/x \tag{17.4}$$

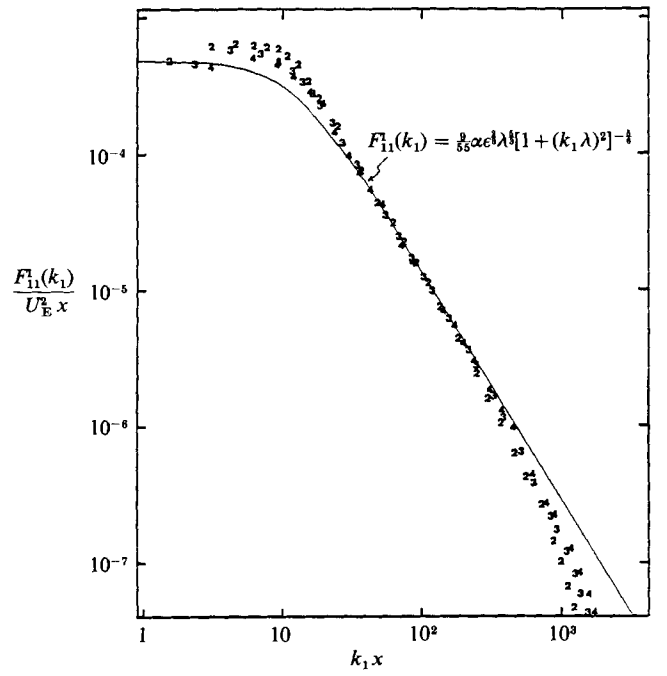

FIGURE 12. Measured one-dimensional spectra of axial velocity (symbol = x/D).

as our best estimate. Using $u \approx 0.16U_E$ yields an estimate for l as

$$l = 0.086x, \tag{17.5}$$

which is close to the integral scale obtained from the streamwise velocity correlation.

We can use (17.4) and (5.3) to calculate the Kolmogorov microscale for the mixing layer as

$$\eta = \left[\frac{1}{0.044}\right]^{\frac{1}{4}}\left[\frac{\nu}{U_E D}\right]^{\frac{3}{4}}\left(\frac{D}{X}\right)^{\frac{3}{4}} x. \tag{17.6}$$

Thus for the data of Khwaja and for the pressure measurements reported in §18, $\eta \approx 0.04$–0.1 mm and $l/\eta \approx 600$–1000. Therefore it is reasonable to expect several decades of inertial subrange in the data. Also, since the hot-wire and pressure probes are substantially larger than η, the spectral roll-off at high wavenumbers will be due to probe-averaging effects.

18. The pressure measurements

An attempt was initially made to collapse the considerable body of pressure-fluctuation spectra that have appeared in the literature in recent years (Planchon 1974; Fuchs 1972; Arndt *et al.* 1974). Although all these gave some indication of the expected $k^{-\frac{7}{3}}$ region, uncertainty about the calibrations and basic flow parameters made definitive statements difficult. Therefore an investigation at the centre of the mixing layer of the aforementioned axisymmetric jet was initiated. Arndt *et al.* (1974), using this facility, reported that at the centre of the mixing layer

$$p' = (\overline{p^2})^{\frac{1}{2}} = 0.0625(\tfrac{1}{2}\rho U_E^2) \quad \text{or} \quad p' = 1.26\rho u^2. \tag{18.1}$$

From the theoretical considerations of Part 1, p' is estimated at $\sim 1.9\rho u^2$, with the

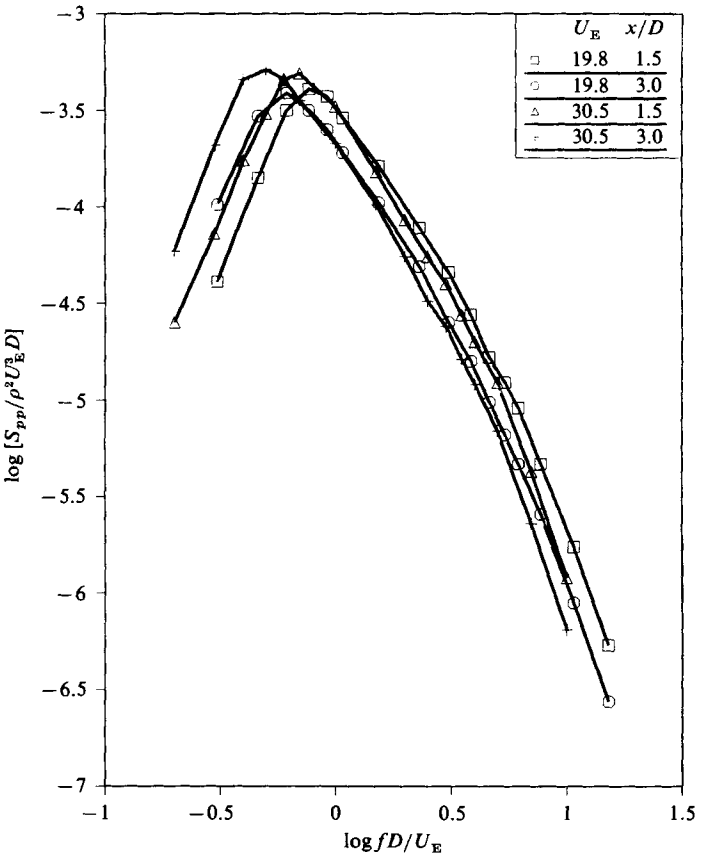

FIGURE 13. Pressure-spectral data normalized by jet exit parameters.

turbulence–mean-shear contribution dominant. If the contribution of this term is reduced by introducing a wavenumber-dependent shear as outlined below, the measured value is obtained.

Spectral measurements were carried out using a Federal Scientific Real-Time Analyzer. The effective bandwidth was 10 Hz and the bandwidth-averaging time product was 400. Spectra were plotted on an (x, y)-plotter as log-spectrum versus frequency, and the data points were read from these plots. An upper limit on the relative spectral error due to averaging and data handling is estimated at 20 %. The measured spectra were corrected for the temporal response of the probe up to a maximum correction of 2 dB. No attempt was made to correct for the limited spatial response nor were data recorded above the spatial cutoff defined earlier.

Spectral measurements were made in the centre of the mixing layer at locations of $x/D = 1.5$ and 3.0, where D is the jet diameter. Exit velocities of 19.8 m/s and 30.5 m/s were used, the lower velocity corresponding to the smallest at which contamination due to background noise was deemed negligible. The Reynolds numbers based on exit velocity and diameter were 4.0×10^5 and 6.2×10^5 respectively. Frequency spectra normalized by only the exit parameters are shown in figure 13.

Wavenumber spectra were computed from frequency spectra by applying the wavenumber-dependent convection velocity of Wills (16.6). The appropriate scaling for the pressure spectra in the range of wavenumbers shown is $F^1_{pp}(k_1)/u^4 l$ versus kl.

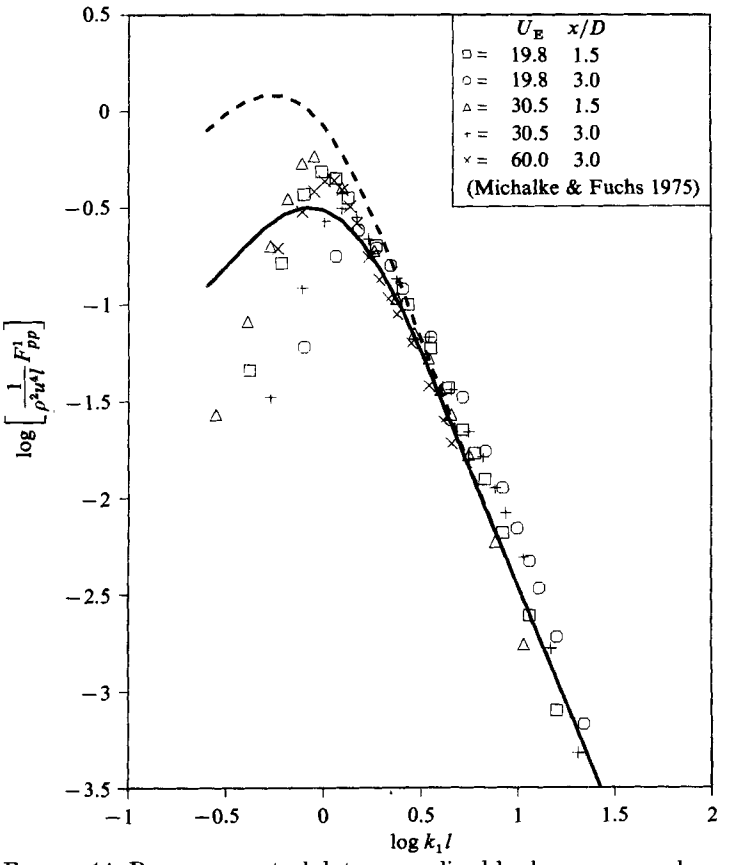

FIGURE 14. Pressure-spectral data normalized by low-wavenumber scaling parameters and calculated spectra.

Spectra normalized in this manner are presented in figure 14. The correction implied by (16.4) was not applied to the data shown.

Also shown in figure 14 are two theoretical spectra computed from the results of §§6 and 7. The dashed-line spectrum is exactly the constant-mean-shear prediction shown in figure 6, where the normalized mean shear has been chosen to equal the maximum shear at the centre of the mixing layer ($Kl/u = 2.95$). Since the jet mixing layer only approximately satisfies the assumptions of constant mean shear and homogeneous turbulence, and then only for the smallest scales, an attempt has been made to compensate for the fact that the larger eddies see an average shear that is somewhat less than the peak centerline value. A wavenumber-dependent mean shear was obtained by first fitting a curve to the mean-velocity profile and then obtaining an average of its derivative between $\pm\pi/k$, or a half-wavelength on each side of the measuring point. This wavenumber-dependent shear was then substituted into the results of tables 1 and 2 to obtain the spectrum shown. As expected, the spectrum at low wavenumbers is reduced. Figure 15 shows the component spectra for the wavenumber-dependent spectrum calculation along with the error spectrum presented in §14.

The spectral data show reasonable collapse for all but the lowest wavenumbers. In view of the large scales (of the order of the distance from the source), the high spectral curvature and the resultant spectral aliasing due to the fluctuating convection

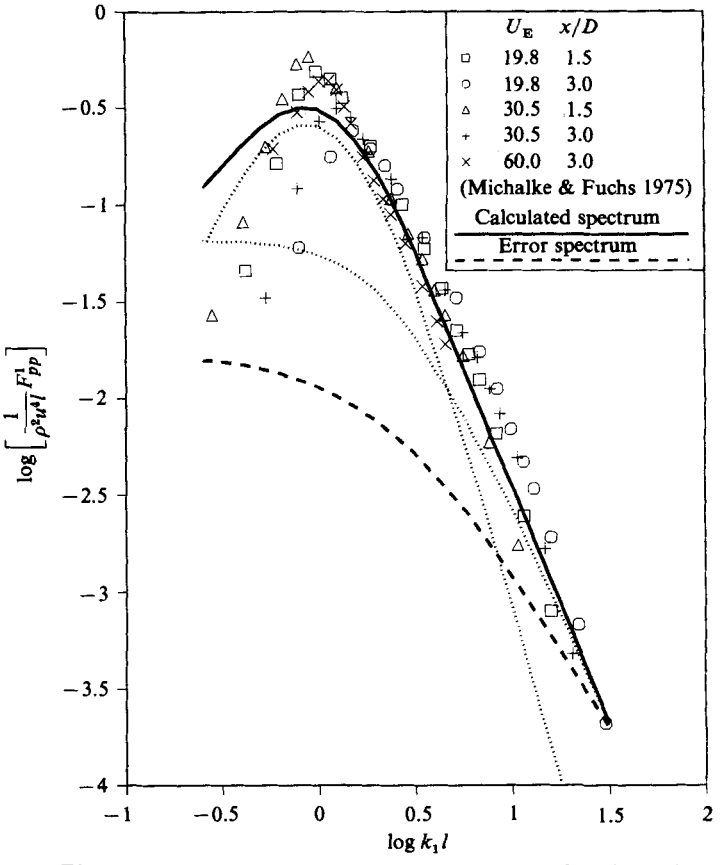

FIGURE 15. *Theoretical pressure spectra based on wavenumber-dependent shear.*

velocity, and in fact the complete breakdown of Taylor's hypothesis, it would have been surprising if the spectra did collapse at these wavenumbers. (Note that this problem does not arise with the velocity spectrum, since it is nearly flat at low wavenumbers.)

There is some evidence of a systematic error in the normalized plots. The accuracy of the jet-exit-velocity determination was only 3–5 %. Also since the measurements were taken at the centre of the mixing layer, where the velocity gradient is a maximum, additional error could have been introduced by a slight mislocation of the probe. Since the velocity enters the scaling in the fourth power, it is reasonable to attribute the observed systematic error to this source.

The values of the constants A and B suggested in §14 were worst-case estimates, and lead to the prediction that the error spectrum should dominate the turbulence–turbulence pressure contribution at nearly all wavenumbers. The lack of a $k^{-\frac{5}{3}}$ range in the experimental data of figure 15 indicates that those values for A and B were too large. The error-spectrum curve shown in figure 15 does not use these worst-case values, but instead assumed values of $A = -0.0075$ and $B = -0.15$. These values are merely upper-limit approximations chosen to be consistent with the data.

The roll-off at high wavenumbers is attributed to the spatial averaging of the probe. At low wavenumbers the spectrum increases as frequency squared. The slope and the peak are taken to indicate that the pressure correlation is negative somewhere (cf. Lumley 1970). This interpretation is consistent with the measured pressure

correlations of Planchon & Jones (1974). The measured spectra of Jones *et al.* (1979) and Michalke & Fuchs (1975) do not continue to fall at low wavenumbers as do these presented here. This difference cannot be attributed to our microphone roll-off, and might be because of a higher background noise in the other facilities.

19. Conclusions

The pressure spectra show reasonable agreement with the theoretical spectra of Part 1 at wavenumbers that correspond to the $k^{-\frac{11}{3}}$ and the $k^{-\frac{7}{3}}$ ranges. While the limited validity of Taylor's hypothesis in this range of wavenumbers and the velocity contamination of the probe clearly have affected the data, the agreement is sufficiently good that the spectral models and the proposed scaling laws can be used with some confidence. Even the fact that the data appear slightly above the theory is what would be expected from the effect of the fluctuating convection velocity on Taylor's hypothesis and the probe errors. The deviations from the theory at low wavenumbers are primarily due to the breakdown of the isotropic assumptions on which the spectral calculations are based.

Particularly striking about the data is the agreement among the various investigators using different techniques. It is clear that, while the phenomenon being measured may not be entirely a pressure fluctuation, it is intrinsic to the device. The agreement with the theoretical results over most of the range presented would seem to provide a strong indication that pressure fluctuations are indeed the dominant influence on the probe. The appearance of a roll-off slower than $k^{-\frac{7}{3}}$ at the higher wavenumbers is consistent with the analysis of §14 and lends credibility to the use of the Siddon–Fuchs equation. The fact that the deviations due to the velocity contamination occur at wavenumbers above that expected indicates that the Siddon–Fuchs estimates of A and B are probably conservative, at least along the centreline of the jet mixing layer.

In view of the fact that few shear flows can be regarded as stronger than the jet mixing layer, it appears unlikely that the $k^{-\frac{11}{3}}$ range arising from the turbulence–mean-shear interaction will be commonly observed. Moreover, since few flows have a turbulence intensity higher than the mixing layer, it seems unlikely that more definitive measurements of the $k^{-\frac{7}{3}}$ range will be made, because of the velocity contamination of the probe. Nonetheless, the measurements and analysis presented in this paper indicate that things may not be as bad as they seem. Since the probe measurement errors are dominant at the higher wavenumbers while the pressure spectra peak strongly at low wavenumbers, reasonably accurate measurements of mean-square pressure fluctuations and low-wavenumber spectra appear to be possible. Moreover, if the $k^{-\frac{7}{3}}$ and $k^{-\frac{11}{3}}$ ranges and the constants suggested are accepted as valid, then a great deal is known about the high wavenumbers, even in the absence of further direct measurements.

The bulk of this paper was first presented at the Acoustical Society of America Meeting in State College, Pa. (July 1977), and subsequently at the American Physical Society/Division of Fluid Dynamics Meetings in Bethlehem, Pa. (November 1977) and at the AIAA Aeroacoustics Meeting in Hartford, Conn. (June 1980).

This work was initiated in 1974 while the authors were at the Applied Research Laboratory of the Pennsylvania State University, and the pressure measurements were carried out in the open-jet facility of that laboratory. The analysis and interpretation has been carried out at the Turbulence Research Laboratory of the

State University of New York at Buffalo and at the Saint Anthony Falls Hydraulic Laboratory of the University of Minnesota. The support of the National Science Foundation under grants ENG 7617466, ATM 7601257 and ATM 7808442 and of the Air Force Office of Scientific Research under contract F4962078-C-0047 is gratefully acknowledged.

The authors would like to express their appreciation to Mrs Eileen Graber for typing numerous drafts of this manuscript and to Mr James Webster for his invaluable assistance in compiling the reference list.

Appendix. The evaluation of (4.6)

We first define $\hat{\mathscr{W}}(\boldsymbol{k})$ to be the Fourier transform of $|\boldsymbol{r}|^{-1}$ given by

$$\hat{\mathscr{W}}(\boldsymbol{k}) \equiv \frac{1}{(2\pi)^3}\int\int\int_{-\infty}^{\infty}\frac{1}{|\boldsymbol{r}|}e^{i\boldsymbol{k}\cdot\boldsymbol{r}}\,d^3\boldsymbol{r}. \tag{A 1}$$

It is obvious that this Fourier transform does not exist in the usual sense. However, if $|\boldsymbol{r}|^{-1}$ is considered to be the limit of a sequence of functions whose Fourier transforms do exist (for example, $|\boldsymbol{r}|^{-1}\exp(-\sigma|\boldsymbol{r}|)$ as $\sigma\to 0$), the Fourier transform *in the sense of generalized functions* can be defined as the limit of these Fourier transforms (see Lighthill 1964; Lumley 1970); the result is

$$\hat{\mathscr{W}}(\boldsymbol{k}) = \frac{1}{2\pi^2 k^2}. \tag{A 2}$$

It is straightforward to show that $W(k)$ from (4.6) can be rewritten as

$$W(\boldsymbol{k}) = \left|\int d\boldsymbol{r}\frac{e^{i\boldsymbol{k}\cdot\boldsymbol{r}}}{|\boldsymbol{r}|}\right|^2 = (2\pi)^6\,\hat{\mathscr{W}}(\boldsymbol{k})\,\hat{\mathscr{W}}(\boldsymbol{k})^*. \tag{A 3}$$

The result of (4.7) follows immediately.

REFERENCES

ARNDT, R. E. A. & NILSEN, A. W. 1971 On the measurement of fluctuating pressure in the mixing zone of a round jet. *ASME Paper* 71-FE-31.

ARNDT, R. E. A., TRAN, N. C. & BAREFOOT, G. L. 1974 Turbulence and acoustic characteristics of screen perturbed jets. *AIAA J.* **12**, 261–262.

BAHNK, T. 1971 Error characteristics of a static pressure probe in isotropic turbulence. B.S. thesis, Dept Aerospace Engng, Pennsylvania State University.

BAREFOOT, G. L. 1972 Fluctuating pressure characteristics in the mixing region of a perturbed and unperturbed round free jet. M.S. thesis, Dept Aerospace Engng, Pennsylvania State University.

BATCHELOR, G. K. 1951 Pressure fluctuations in isotropic turbulence. *Proc. Camb. Phil. Soc.* **47**, 359–374.

BATCHELOR, G. K. 1953 *The Theory of Homogeneous Turbulence.* Cambridge University Press.

BEUTHER, P. D., GEORGE, W. K. & ARNDT, R. E. A. 1977*a* Modeling of pressure spectra in a turbulent shear flow. *Am. Acoust. Soc. Meeting Paper, State College, Pa.*

BEUTHER, P. D., GEORGE, W. K. & ARNDT, R. E. A. 1977*b* Pressure spectra in a turbulent shear flow. *Bull. Am. Phys. Soc.* **22**, 1285.

BRADSHAW, P., FERRIS, D. H. & JOHNSON, R. F. 1964 Turbulence in a noise-producing region of a round free jet. *J. Fluid Mech.* **19**, 591–624.

CHANDRASEKHAR, S. 1949 On Heisenberg's elementary theory of turbulence. *Proc. R. Soc. Lond.* A **200**, 20–33.

CORRSIN, S. 1951 The decay of isotropic temperature fluctuations in an isotropic turbulence. *J. Aero. Soc.* **18**, 417–423.

DAVIES, P. O. A. L., FISCHER, M. J. & BARRETT, M. J. 1963 The characteristic of the turbulence in the mixing layer of a round jet. *J. Fluid Mech.* **15**, 337–367.

DUTTON, J. A. & DEAVEN, D. C. 1972 Some properties of atmospheric turbulence. In *Statistical Models and Turbulence* (ed. M. Rosenblatt & C. W. Van Atta). Lecture Notes in Physics, vol. 12, pp. 402–406. Springer.

ELLIOT, J. A. 1972 Microscale pressure fluctuations measured within the lower atmospheric boundary layer. *J. Fluid Mech.* **3**, 351–383.

FRENKIEL, F. N. & KLEBANOFF, P. S. 1966 Space–time correlations in turbulence. In *Dynamics of Fluids and Plasmas* (ed. S. I. Pai). Academic.

FUCHS, H. V. 1970 Über die Messung von Druck-Schwankungen mit umströmten Mikrofonen in Freistrahl. *DFVLR Tech. Rep.* DLR-FB70-22.

FUCHS, H. V. 1972 Measurement of pressure fluctuations within subsonic turbulent jets. *J. Sound Vib.* **22**, 361–378.

GEORGE, W. K. 1974 The equilibrium range of turbulent pressure spectra. *Bull. Am. Phys. Soc.* **19**, 1158.

GEORGE, W. K. & BEUTHER, P. D. 1977 Pressure spectra in a homogeneous isotropic turbulent flow. *Bull. Am. Phys. Soc.* **22**, 1285.

GEORGE, W. K., BEUTHER, P. D. & ARNDT, R. E. A. 1980 Pressure spectra in turbulent free shear flows. *AIAA Aero. Meeting Paper* 80–0985, *Hartford, Conn.*

GOLITZIN, G. S. 1964 Time spectrum of micro-fluctuations in atmospheric pressure. *Izv. Akad. Nauk SSSR, Ser. Geofiz.* **8**, 1253–1258.

GOSSARD, E. E. 1960*a* Power spectra of temperature, humidity, and refractive index from aircraft and tethered balloon measurements. *Trans. Inst. Radio Engrs on Antennas and Propagation* AP-8, 186–201.

GOSSARD, E. E. 1960*b* Spectra of atmospheric scalars. *J. Geophys. Res.* **65**, 3339–3351.

HEISENBERG, W. 1948 Zur statischen Theorie der Turbulenz. *Z. Phys.* **124**, 628–657.

HINZE, J. D. 1959 *Turbulence, An Introduction to its Mechanism and Theory.* McGraw-Hill.

IGARASHI, J. & FUJISAMA, A. 1968 Space and time correlation of the pseudo-pressure field. *6th Intl Congr. Acoust., Paper* F-4-4.

INOUE, E. 1954 The application of turbulence theory to oceanography. *J. Met. Soc. Japan* **28**, 441–456.

JONES, B. G., ADRIAN, R. J., NITHIANANDAN, C. K. & PLANCHON, H. P. 1979 Spectra of turbulent static pressure fluctuations in jet mixing layers. *AIAA J.* **17**, 449–457.

KHWAJA, M. S. 1980 Spectral characteristics of the jet mixing layer. MS thesis, Dept Mech. Engng, State University of NY at Buffalo.

KOBASHI, Y. 1957 Measurements of pressure fluctuation in the wake of a cylinder. *J. Phys. Soc. Japan* **12**, 533.

KOBASHI, Y., KONO, N. & NISHI, T. 1960 Improvement of a pressure pick-up for the measurements of turbulence characteristics. *J. Aero. Sci.* **27**, 149.

KOLMOGOROV, A. 1941 The local structure of turbulence in incompressible viscous fluid for very large Reynolds numbers. *C.R. Acad. Sci. URSS* **30**, 301–305.

KRAICHNAN, R. H. 1956 Pressure field within homogeneous anistropic turbulence. *J. Acoust. Soc. Am.* **28**, 64.

LIGHTHILL, M. J. 1964 *An Introduction to Fourier Analysis and Generalized Functions.* Cambridge University Press.

LILLEY, G. M. 1958 On the noise from air jets. *ARC Rep.* 20.

LUMLEY, J. L. 1965 Interpretation of time spectra measured in high intensity shear flows. *Phys. Fluids* **8**, 1056–1062.

LUMLEY, J. L. 1970 *Stochastic Tools in Turbulence.* Academic.

MACKAWA, T. 1965 Pressure fluctuation measuring apparatus with condenser microphone. In *Proc. 15th Japanese Natl Congr. Appl. Mech.*

MICHALKE, A. & FUCHS, H. V. 1975 On turbulence and noise of an axisymmetric shear flow. *J. Fluid Mech.* **70**, 179–205.

MIKKELSEN, T. 1978 Unpublished data of Risø 1978 experiment.

MIKSAD, R. W. 1976 Omni-directional static pressure probe. *J. Appl. Met.* **15**, 1215–1225.

MILLIONSHCHIKOV, M. D. 1941 Theory of homogeneous isotropic turbulence. *Izv. Akad. Nauk SSSR, Ser. Geofiz.* **5**, 433–446.

MONIN, A. S. & YAGLOM, A. M. 1975 *Statistical Fluid Mechanics*, vol. II. MIT Press.

OBUKHOV, A. M. 1949 Pressure fluctuations in a turbulent flow. *Dokl. Akad. Nauk SSSR, Ser. Geofiz.* **3**, 49–68.

OBUKHOV, A. M. & YAGLOM, A. M. 1951 Microstructure of a turbulent jet flow. *Prikl. Mat. Mekh.* **15**, 3–26.

PAO, Y. H. 1965 Structure of turbulent velocity and scalar fields at large wavenumbers. *Phys. Fluids* **8**, 1063–1075.

PLANCHON, H. P. 1974 The fluctuating static pressure field in a round jet mixing region. Ph.D. thesis, University of Illinois.

PLANCHON, H. P. & JONES, B. G. 1974 A study of the local pressure field in turbulent shear flow and its relation to aerodynamic noise generation. In *Proc. 2nd Interagency Symp. on University Res. in Trans.*, vol. 1, pp. 21–35.

REYNOLDS, W. C. 1976 Computation of turbulent flows. *Ann. Rev. Fluid Mech.* **8**, 183–208.

ROUSE, H. 1953 Cavitation in the mixing zone of a submerged jet. *Houille Blanche* **8**, 9.

SAMI, S., CARMODY, T. & ROUSE, H. 1967 Jet diffusion in the region of flow establishment. *J. Fluid Mech.* **27**, 231–252.

SIDDON, T. E. 1969 On the response of pressure measuring instrumentation in unsteady flow. *Univ. Toronto Inst. Aerospace Rep.* 136.

SPENCER, B. W. 1974 Statistical investigation of turbulent velocity and pressure fields in a two stream mixing layer. Ph.D. dissertation, University of Illinois at Urbana.

SPENCER, B. W. & JONES, B. G. 1971 A bleed-type pressure transducer for in-stream measurement of static pressure fluctuations. *Rev. Sci. Instrum.* **42**, 450–454.

STRASBERG, M. 1963 Measurements of fluctuating static and total head pressure in a turbulent wake. *AGARD Rep.* 464.

TAYLOR, G. I. 1935 Statistical theory of turbulence. IV. Diffusion in a turbulent air stream. *Proc. R. Soc. Lond.* A **151**, 465–478.

TAYLOR, G. I. 1936 Statistical theory of turbulence. V. Effect of turbulence on boundary layer. *Proc. R. Soc. Lond.* A **156**, 307–317.

TENNEKES, H. & LUMLEY, J. L. 1972 *A First Course in Turbulence.* MIT Press.

TOWNSEND, A. A. 1976 *The Structure of Turbulent Shear Flow*, 2nd edn. Cambridge University Press.

TRAN, N. 1972 Turbulence characteristics in the mixing region of a perturbed and unperturbed round free jet. M.S. thesis, Dept Aerospace Engng, Pennsylvania State University.

UBEROI, M. S. 1953 Quadruple velocity correlations and pressure fluctuations in isotropic turbulence. *J. Aero. Sci.* **20**, 197–204.

VAN ATTA, C. W. & WYNGAARD, J. C. 1975 On higher-order spectra of turbulence. *J. Fluid Mech.* **72**, 673–694.

VON FRANK, E. 1970 Turbulence characteristics in the mixing region of a perturbed and unperturbed round free jet. MS thesis, Dept Aerospace Engng, Pennsylvania State University.

VON KÁRMÁN, T. 1948 Progress in the statistical theory of turbulence. *Proc. Natl Acad. Sci. USA*, **34**, 530–539.

WILLMARTH, W. W. 1975 Pressure fluctuation beneath turbulent boundary layers. *Ann. Rev. Fluid Mech.* **7**, 13–38.

WILLS, J. A. B. 1964 On convection velocities in turbulent shear flows. *J. Fluid Mech.* **20**, 174–432.

WYNGAARD, J. C. & CLIFFORD, S. F. 1975 Taylor's hypothesis and high frequency turbulence spectra. *J. Atmos. Sci.* **34**, 922–929.

YAGLOM, A. M. 1949 Acceleration field in a turbulent flow. *Dokl. Akad. Nauk SSSR* **67**, 795–798.